Compositions of dust and sea salts in the Dome C and Dome Fuji ice cores from Last Glacial Maximum to early Holocene based on ice-sublimation and single-particle measurements

I. Oyabu[*,1,2,3], Y. Iizuka[2], K. Kawamura[1,4,5], E. Wolff[6], M. Severi[7], R. Ohgaito[8], A. Abe-Ouchi[9,1,8], and M. Hansson[3]

[1]National Institute of Polar Research, Research Organization of Information and Systems, Tokyo 190-8518, Japan. [2]Institute of Low Temperature Science, Hokkaido University, Sapporo 060-0819, Japan. [3]Department of Physical Geography, Stockholm University, Stockholm 106 91, Sweden. [4]Department of Polar Science, The Graduate University of Advanced Studies (SOKENDAI), Tokyo 190-8518, Japan. [5]Japan Agency for Marine Science and Technology (JAMSTEC), Yokosuka 237-0061, Japan. [6]Department of Earth Sciences, University of Cambridge, Cambridge CB2 3EQ, UK. [7]Department of Chemistry "Ugo Schiff", University of Florence, Italy. [8]Japan Agency for Marine-Earth Science and Technology, Yokohama, 236-0001, Japan. [9]Atmosphere Ocean Research Institute, University of Tokyo, Kashiwa, Chiba 277-8564, Japan

*Corresponding author: Ikumi Oyabu (oyabu.ikumi@nipr.ac.jp)

Key Points:

- Dust flux in the Dome C core is significantly lower than in the Dome Fuji core from the LGM to the early Holocene
- Comparison of dust size and aspect ratio between the two cores suggest dominance of Patagonian dust source during the LGM
- Most Cl was lost to the atmosphere from snow at Dome C, while it was preserved at Dome Fuji as NaCl and in solid solution in the Holocene

Abstract

We analyzed the chemical compositions of dust and sea-salt particles in the EPICA Dome C (EDC) ice core during 26–7 kyr BP using an ice-sublimation technique, and compared the results with existing data of the Dome Fuji (DF) ice core. Combined with ion concentration data, our data suggested similar sea-salt fluxes in both cores and significantly lower dust flux in the EDC core. The differences in modal size and aspect ratio of dust particles between the two cores support the dominance of Patagonian source suggested by earlier works. The compositions of calcic dust showed major change at ~17 kyr BP, possibly reflecting a relative increase in dust transported via the upper troposphere. The calcium sulfate fraction was higher in the DF core than in the EDC core after ~17 kyr BP, suggesting that higher Patagonian dust contribution to the DF region. Abundant NaCl particles were found in the DF core in comparison with the EDC core from the LGM to early Holocene, possibly because of the high concentration of terrestrial dust in the DF core that reduced acid availability for sea-salt modification. During the Holocene, the lower NaCl fraction and Cl^-/Na^+ ratio in the EDC core suggested that most Cl^- was lost to the atmosphere from snow at Dome C, while it was preserved at Dome Fuji as NaCl and solid solution.

1 Introduction

Aerosols affect climate through direct and indirect effects, and radiative forcings associated with these effects depend on the size and type of aerosol particles, their atmospheric concentrations, chemical compositions, and mixing states (IPCC, 2007, 2013). Terrestrial dust supplies nutrients such as iron (Fe) to the ocean, and may play a significant role in marine biological activity and thus uptake of atmospheric CO_2 (Martin et al., 1990; Martínez-Garcia et al., 2011). Sea-salt particles represent the major source of chlorine (Cl) in the atmosphere over the Southern Ocean and Antarctica and they play an important role in the biogeochemical cycling of halogens (Vogt et al., 1996).

Antarctic ice cores contain impurities that originate from terrestrial dust and sea salts, and these have been extensively used for the reconstruction of past atmospheric aerosol content and transport, environment in source regions, and chemistry in atmosphere and snow (e.g., Petit et al., 1999; Watanabe et al., 2003a; Wolff et al., 2006, 2010; Fischer et al., 2007; Lambert et al., 2008, 2012; Dome Fuji Ice Core Project Members, 2017; Goto-Azuma et al., 2019).

The concentrations of insoluble particles and non-sea-salt calcium ($nssCa^{2+}$) in melted ice-core samples, as well as total concentrations of elements such as Al, Fe, and Ca, have commonly

been used as proxies for terrestrial dust (e.g., Legrand & Mayewski, 1997; Röthlisberger et al., 2000; Delmonte et al., 2002; Bigler et al., 2006, 2011; Fischer et al., 2007; Lambert et al., 2008; Ruth et al., 2008; Sato et al., 2013; Dome Fuji Ice Core Project Members, 2017). The dust flux during glacial maxima in East Antarctica was one order of magnitude higher than during interglacial periods (Lambert et al., 2008; Dome Fuji Ice Core Project Members, 2017), probably because of the combinations of variations in dust emissions, dust source areas, atmospheric transport efficiency, and scavenging during long-range transport (Wolff et al., 2006, 2010; Fischer et al., 2007; Sugden et al., 2009; Delmonte et al., 2017).

Few studies have investigated the regional differences in dust flux. In East Antarctica, the nssCa^{2+} flux in the Last Glacial Maximum (LGM) was about 3 times higher in the EPICA Dronning Maud Land (EDML) ice core than in the EPICA Dome C (EDC) ice core (Fig. 1, Fischer et al., 2007). The difference may reflect the proximity of these sites to southern South America, the major dust source during the LGM (e.g., Grousset et al., 1992; Basile et al., 1997; Delmonte et al., 2004b, 2008; Mahowald et al., 2006). Model simulations have supported this view (Li et al., 2008; Albani et al., 2012; Neff & Bertler, 2015; Ohgaito et al., 2018). However, the spatial distribution of dust deposition fluxes has not been well established because of the uncertainty associated with quantitative comparison of data sets obtained by different laboratories and different techniques. For example, published insoluble dust flux at EDC is several times higher than at Dome Fuji (DF) throughout the past 720 kyr (Lambert et al., 2008; Dome Fuji Ice Core Project Members, 2017). This appears puzzling especially for glacial maxima, considering the distances of the core sites from southern South America. The nssCa^{2+} flux in the EDC core during the LGM (Wolff et al., 2006) was ~65% that of the DF core (Oyabu et al., 2014), contradicting with the insoluble dust records [note, however, that calcic dust only represents a small (and variable) fraction (~1/10 to ~1/100) of total terrestrial dust (Lambert et al., 2012)].

Chemical compositions of calcic dust might provide information about transport pathways, especially in terms of altitude. Calcium nitrate ($Ca(NO_3)_2$) and calcium sulfate ($CaSO_4$) are produced by chemical reactions between calcium carbonate ($CaCO_3$) and nitric acid (HNO_3) or sulfuric acid (H_2SO_4) in the atmosphere (Legrand et al., 1997; Gibson et al., 2006; Mahalinganathan & Thamban, 2016). Legrand et al. (1988) suggested that nitrate (sulfate) might be transported through the upper and mid-troposphere (marine boundary layer) because the major sources of atmospheric HNO_3 are in the mid- to upper troposphere and stratosphere (Wolff, 1995; Savarino et al., 2007), while the source of H_2SO_4 is dimethyl sulfide emitted from the sea (Davis et al., 1998).

Sodium chloride (NaCl) undergoes acid displacement reactions with H_2SO_4, HNO_3, and methanesulfonic acid (MSA) in the atmosphere to release hydrochloric acid (HCl) and deplete Cl in

sea salts (Newberg et al., 2005 and references therein). After deposition of sea salts onto the ice-sheet surface, the reactions may occur also in the snowpack (Röthlisberger et al., 2003), and the released HCl may escape to the atmosphere or remain in the snow and preserved. Thus, the chemical compositions and relative abundances of sea-salt particles in ice cores are thought to provide constraints on the magnitude of Cl depletion in sea-salt aerosols in the past atmosphere and snow.

For deep ice cores covering glacial–interglacial timescales, earlier studies have provided inconsistent data and interpretations on the sea-salt composition in the Antarctic interior. The Cl^-/Na^+ ratio was close to (significantly lower than) the seawater ratio in the EDC core during the LGM (Holocene), suggesting little (substantial) modification of sea salts (Röthlisberger et al., 2003). For the DF core during the LGM, however, Iizuka et al. (2008) suggested that about half the sea salt was Na_2SO_4 even though Cl^-/Na^+ was close to the seawater ratio (thus substantial existence of HCl), based on the considerations of ion balance and preferences of chemical reactions (e.g., $CaCO_3$ reacts more readily than NaCl with H_2SO_4). The elemental analyses of individual microparticles in the DF core also supported this conclusion (Oyabu et al., 2014). On the other hand, Cl^-/Na^+ in the DF core during the Holocene is comparable with or even higher than the seawater ratio (Watanabe et al., 2003a), suggesting either little sea-salt modification or preservation of HCl in ice (Domine & Thibert, 1995a). The latter explanation was preferred from the ion balance and preference of chemical reactions (Iizuka et al., 2008). However, Oyabu et al. (2014) found a significant fraction of NaCl particles (~1/4 of all sea-salt particles) for the latter part of the last Termination and early Holocene from the direct observation of particles, and demonstrated that NaCl particles are able to reach the Antarctic inland and be preserved without modification. This illustrates the importance of direct measurements of individual particle compositions to accurately determine the abundance of sea salts and acids in the ice cores.

Simultaneous measurements of the chemical compositions of dust and sea-salt particles may provide invaluable information about past atmospheric circulation, transport processes, and chemistry. Iizuka et al. (2009) developed such a method, in which nonvolatile particles (in both soluble and insoluble forms) are extracted from an ice sample by sublimating ice and their elemental constituents are measured using a scanning electron microscope (SEM) and an energy dispersive X-ray spectrometer (EDS) (hereafter, sublimation-EDS). Based on this method, previous studies have discussed the compositions and concentrations of sulfate and chloride salts in the DF core (Iizuka et al., 2012a; Oyabu et al., 2014) and Talos Dome core (Fig. 1, Iizuka et al., 2013), as well as the modification of modern sea-salt particles from surface snow measurements (Iizuka et al., 2012b, 2016). However, the chemical compositions of most dominant particles, i.e., insoluble particles containing silicate, have not been the focus of the previous research. Moreover, as the

sublimation-EDS method is relatively new and it has been applied only to the above-mentioned ice cores, it is desirable to apply it to other ice cores both to improve the understanding of the spatial variability of aerosol compositions and to investigate their causes.

Here, we present the first comparison of the chemical compositions of nonvolatile particles including both terrestrial dust and sea salts between two inland dome cores in East Antarctica (EDC and DF) using the same analytical methods. The geographical setting of Dome C is similar to Dome Fuji in terms of distance from the nearest coast, i.e., ~950 and ~930 km for EDC and DF, respectively (Fig. 1), and both sites are on local dome summits (Watanabe et al., 2003b; EPICA Community Members, 2004). The patterns of temporal variations in water isotope and insoluble dust records are similar to each other (Jouzel et al., 2007; Lambert et al., 2012; Dome Fuji Ice Core Project Members, 2017). However, the deposition fluxes and chemical compositions of terrestrial dust and sea salts may be different because of environmental differences such as the distance from the major dust sources and air masses reaching the core sites with different trajectories and durations. By comparing sublimation-EDS data from the two ice cores from the LGM to the early Holocene, we discuss the differences in total dust flux (including both soluble and insoluble dust), transport pathways of dust, and modifications of sea-salt particles.

2 Method

2.1 Experimental procedure of the sublimation-EDS method

The EDC ice core samples used in this study had been stored in the cold storage facility at the Institut des Géosciences de l'Environnement (IGE, formerly LGGE, Grenoble, France). We selected 30 samples at approximately regular time intervals from 222.75 m (Middle Holocene: 6.8 kyr BP) to 570.50 m (LGM: 26.3 kyr BP). Each sample (length: 10 cm along with the depth of core, cross section: 3 × 2 cm) was cut from a 55-cm section at IGE. The samples were then transported to a cold laboratory at the Department of Physical Geography, Stockholm University where they were stored at −25 °C until sublimation treatment.

We employed the experimental method developed by Iizuka et al. (2009); thus, only a brief description is given here. The method extracts nonvolatile particles (in both soluble and insoluble forms) from an ice sample by exposing it to a flow of cold dry air that sublimates the ice and volatile materials. The sublimation system employed in this study (constructed at Stockholm University) comprised an air compressor, air filters, sublimation chamber, and chest freezer, placed in a normal laboratory room (not a clean room).

159 The surface of each sample was first shaved off by 1–2 mm using a clean ceramic knife for
160 decontamination. Then, about 1 g of ice was shaved off from the 7–10-cm-long cleaned surface with
161 the knife and was placed on a polycarbonate membrane filter (ADVANTEC®, K040A013A, pore
162 size: 0.40 μm, diameter: 13 mm) fixed in the stainless-steel sublimation chamber by using a
163 polypropylene funnel. The chamber was then sealed in a plastic laboratory bottle precleaned with
164 ultrapure water and ethanol. Great care was taken to exclude contamination from particles in the cold
165 room, by handling the ice samples and sublimation chambers in a clean booth with precleaned tools
166 (the sublimation chamber, ceramic knife, funnel, and tweezers for handling filter were cleaned with
167 ethanol after each use). The laboratory bottle was placed in an insulated box and brought out from
168 the cold room to the sublimation system, and the sublimation chamber was quickly taken out from
169 the bottle and connected to the fittings inside the chest freezer. Clean air generated using an oil-free
170 air compressor and a particle filter (pore size: 0.03 μm) flowed through a 5-m-long tube and the
171 sublimation chamber placed in the freezer at −50 °C to sublimate ice and volatile materials. The ice
172 sublimation was completed within 100 hours at a flow rate of 15 L min^{-1}. After sublimation, the
173 sublimation chamber was brought to the cold room in a cleaned plastic bottle. The membrane filter
174 was taken out of the sublimation chamber and placed in a stainless-steel laboratory dish (with a lid)
175 precleaned with ethanol. The dish was further sealed in a particle-free plastic bag to minimize its
176 exposure to atmosphere, and brought to room temperature for storage at Stockholm University for up
177 to two months.

178 The sample filters were then transported in a plastic container designed for keeping the
179 filters upright, and further sealed in a Tupperware, and hand-carried on passenger flights and trains
180 to the Institute of Low Temperature Science (ILTS) Hokkaido University, Japan. There, each sample
181 filter was coated with a Pt film to avoid electrical charging of the filter, and sealed again in a
182 stainless-steel dish with lid and particle-free plastic bag, and stored in a desiccator until analyses.
183 The SEM (JEOL JSM-6360LV) - EDS (JEOL JED2201) is installed in a normal laboratory room
184 (not a clean room); thus, care was taken not to introduce microparticle contaminations to the samples
185 (Iizuka et al., 2009). The sample filters were placed on a Cr sample holder and capped by a
186 stainless-steel lid in a clean booth, and then placed on the sample stage of SEM. The lid was
187 removed from the sample just before inserting it into the vacuum chamber of SEM.

188 The elemental composition was analyzed using EDS in a point-analysis mode with beam
189 diameter of 64 nm (JEOL JED2201). We measured particles larger than 0.5 μm of the longest
190 diameter because of the limitation of the filter size (0.4 μm) and the analytical resolution of the EDS
191 system. An accelerating voltage of 20 kV was used to observe the elemental compositions on the
192 surface as well as within the particles. The X-ray spectrum of each particle was measured for 45–80

s to detect atomic ratios. The reproducibility of the atomic ratio for each element was ~40%. All data including atomic ratios are shown in the Appendix (Figs. A1 and A2).

The instrument also detected C, O, Cr, and Pt but they contained artifacts from the membrane filter (C, O), sample mount (Cr), and filter coating (Pt); thus, they were not used for calculating the elemental ratios. We performed blank tests of the entire system by operating it without ice and we only found three to five particles containing C and O in each test; thus, contamination from the sublimation system was considered negligible. During the actual ice-core measurements, we found some large particles (larger than ~8 μm) with sharp corners and a strong Fe peak in the EDS spectrum, which were probably fragments of the sublimation chamber. As they are distinct from natural microparticles, we interrupted the EDS measurements after a few seconds for such particles. Fe was also detected in some particles mostly in combination with Si, and a single Fe peak was found in a few particles (<2% of all particles for each ice sample). We considered this as natural Fe in the terrestrial dust and thus included such data for the analyses of elemental ratios. Approximately 200 particles were randomly selected from all the particles on each filter (more than 400 and up to several thousands). In this study, 6105 particles from 30 ice samples were analyzed.

Area (A), maximum Feret diameter ($D_{Feret\ max}$) and minimum Feret diameter ($D_{Feret\ min}$) of each particle were analyzed with an image processing program (ImageJ, Schindelin et al., 2012). Feret diameter (also known as caliper diameter) is defined as the distance between two parallel tangents of the particle. Circular equivalent diameter (D_{circ}) and aspect ratio (AR) were then calculated as follows.

$$D_{circ} = 2 \times \sqrt{A/\pi} \quad (1)$$

$$AR = \frac{D_{Feret\ max}}{D_{Feret\ min}} \quad (2)$$

We note that the chemical compositions of the particles are not altered by reactions with acids in the ice during the sublimation process because of both the low temperature (−50 °C) and low probability of contact between the particles and acids (Iizuka et al., 2009; Oyabu et al., 2014, 2015). This was confirmed through previous studies on the DF core; the composition and abundance of soluble salt particles (mainly Na_2SO_4 and $CaSO_4$) measured directly using Raman spectroscopy (Ohno et al., 2005, 2006; Sakurai et al., 2011) agreed well with those measured using the sublimation-EDS method for the LGM, last Termination, and Holocene (Iizuka et al., 2012a; Oyabu et al., 2014).

2.2 Other data sets and chronology

We used published Ca^{2+}, Na^{+}, SO_4^{2-}, Cl^{-} and NO_3^{-} ion concentration data of the EDC ice core (Littot et al., 2002; Wolff et al., 2006) to interpret our sublimation-EDS results. Briefly, Ca^{2+}, Na^{+}, SO_4^{2-}, Cl^{-} and NO_3^{-} concentrations were measured from the surface to the depth of 788 m with ~5-cm resolution (2.5 cm for some sections) at five laboratories (i.e., the University of Florence, Stockholm University, British Antarctic Survey, IGE, and University of Copenhagen) using ion chromatography (IC). Inter-laboratory comparison of the two Holocene ice samples revealed that Ca^{2+} concentration varied by about ±30%, that Na^{+} and Cl^{-} concentrations varied by about ±10% and NO_3^{-} concentration varied by > ±50% (but routine ice-core NO_3^{-} analyses show better agreements) among the five laboratories (Littot et al., 2002).

We also used published data from the DF core. These comprised elemental compositions of nonvolatile particles derived using the sublimation-EDS method (Oyabu et al., 2014), Na^{+}, Ca^{2+}, SO_4^{2-}, and Cl^{-} concentrations obtained by IC (Oyabu et al., 2014), and total Al and Na concentrations derived using the full-digestion method (Sato et al., 2013) from the LGM to the early Holocene, as well as the average NO_3^{-} concentration for the early Holocene and LGM (Goto-Azuma et al., 2019). The sublimation-EDS measurements were performed at ILTS on 47 samples (295.0–579.8 m corresponding to 9.4 – 25.2 kyr BP) with mean resolution of ~300 yr. Of 47 samples in Oyabu et al. (2014), we reanalyzed 28 of particle images in this study. The IC measurements were performed at National Institute of Polar Research (NIPR) on 144 samples (298.9 – 580.6 m) with ~100-yr resolution, and NO_3^{-} was also measured at NIPR. The full-digestion treatments were performed at Yamagata University and the sample measurements were performed at NIPR on the same 144 samples as the IC measurements.

We placed the above data sets on the AICC2012 age scale (Veres et al., 2013). Adopting AICC2012 for the EDC data is straightforward because the EDC core was originally included in the construction of AICC2012. Published volcanic synchronization between the EDC and DF cores (Fujita et al., 2015) was used to convert the DF chronology to AICC2012.

Surface mass balance (SMB) data at EDC and DF are required for deducing ion fluxes onto the respective sites. We used recent SMB data at EDC based on the relationship between the hydrogen isotopic ratio corrected for mean oceanic isotopic ratio, vapor source temperature, and accumulation rate (Parrenin et al., 2016). For deducing SMB at DF, we used the ratio of SMB between the two sites based on the volcanic synchronization of the ice cores (Fujita et al., 2015; Parrenin et al., 2016).

3 Results

3.1 Chemical constituents of observed particles

We classify the measured particles into four categories: "terrestrial dust," "sea salts," "mixture of terrestrial dust and sea salts," and "others/unknown," according to the combinations of detected elements, which are consistent with previous works for the DF, Talos Dome and NEEM (Greenland) ice cores (Iizuka et al., 2009, 2012a, 2012b, 2013, 2016; Oyabu et al., 2014, 2015) (Fig. 2). Below, we describe the typical particle compositions for each classification and discuss the uncertainties associated with possible misclassifications.

(i) Terrestrial dust

- Si, Al, and/or Ti with neither S nor Cl (e.g., Fig. 3a, c).
- Si and Na.
- Ca without Na (e.g. $CaSO_4$, $CaCl_2$, $Ca(NO_3)_2$, and $CaCO_3$).

(ii) Sea salt

- Na (and/or Mg) and Cl with neither Si nor Ca (NaCl and/or $MgCl_2$).
- Na and S with neither Si nor Ca (Na_2SO_4) (e.g., Fig. 3b, e).
- Na only ($NaNO_3$).

(iii) Mixture of terrestrial dust and sea salt

- Na, one of or both Si and Ca, and one of or both Cl and S (e.g., Fig. 3a, d).

(iv) Others/unknown

- Minor particles not classified above, mostly containing combinations of Mg and S, K and S, or K and Cl, without Na and Ca, as well as those containing only S, Cl, or one of the following combinations: S and Si, S and Al, S and Fe, Cl and Si, Cl and Al, or Cl and Fe. Their sources are unknown or difficult to attribute explicitly to marine or terrestrial environments. Their total fraction accounts for only < 5 % of all measured particles.

We note that our scheme inevitably misclassifies particles that can be interpreted as both terrestrial and sea-salt particles; thus, the results have inherent uncertainties as follows.

(1) A mixture of terrestrial dust and $NaNO_3$ (modified sea salt) is classified as "terrestrial dust" because nitrate is not measured. This misclassification should not introduce large uncertainty to the number fractions because there are only 5 particles that contain only Na ($NaNO_3$ without dust) while particles containing only Na and S (Na_2SO_4 without dust) and Na and Cl (NaCl without dust) are abundant (1111 and 97 particles, respectively) among the ~6000 measured

particles.

(2) Particles containing Fe and S or those containing Fe and Cl (both without Si) are classified as "others/unknown," but they might be terrestrial dust particles. Such particles account for only 0.5 % of all particles and therefore introduce little uncertainty.

(3) All particles containing Ca are classified as terrestrial dust, although frost flowers (on sea ice) can produce calcium salts such as $CaCO_3$ and $CaSO_4$ (Sala et al., 2008; Geilfus et al., 2013), and sea spray is also a potential source of calcium compounds (Salter et al., 2016). The mass of $ssCa^{2+}$ during the LGM is smaller than that of sea-salt (ss) Na^+ by a factor of 20–50 (Bigler et al., 2006; Hara et al., 2017). Considering that $ssNa^+$ flux is comparable to $nssCa^{2+}$, the overestimation of terrestrial dust introduced by $ssCa^{2+}$ particles would be < ~10 % (based on Ca mass) during the LGM. On the other hand, the analysis of the Ca^{2+} and Na^+ concentrations of the EDC core suggests that about 50 % of Ca^{2+} in the Holocene is $ssCa^{2+}$ (Bigler et al., 2006). Similar analysis of the DF core using published ion data (Oyabu et al., 2014) suggests that the $ssCa^{2+}$ represents ~20 % of the Ca^{2+}. Thus, the terrestrial Ca particle fraction might be overestimated in the Holocene. However, the fraction of the relevant Ca-containing particles is only 14 and 10 % of all the particles in the Holocene for the EDC and DF cores, respectively. Thus, the error associated with ssCa does not affect our main conclusion on dust flux comparison (Section 4.1).

(4) All particles containing Na and either Cl or S are classified as sea salts, but some of them could originate in terrestrial dust. For example, a particle containing Na, Mg, Al, Si, S, K, Ca and Fe is classified as a mixture of terrestrial dust and sea salts (a combination of Na_2SO_4, $CaSO_4$, and silicate minerals), although it might be a mixture of terrestrial components (including $CaSO_4$ and $NaAlSi_3O_8$). Also, terrestrial halide and marine clay include NaCl and they might represent major sources of nssNa especially during the LGM (Bigler et al., 2006). Nevertheless, their compositions are indistinguishable from sea salts, thus they are classified as sea-salt or mixed particles.

To examine the possible magnitude of the misclassification regarding (4) above (Na in terrestrial dust), we estimated the mass fractions of Na in the terrestrial dust, sea-salt, and mixed particles based on our EDS data. They were then compared with the ratio of ssNa to total Na deduced from two published datasets: ion measurement for soluble Na of the EDC core (Littot et al., 2002; Wolff et al., 2006) and that of the DF core (Oyabu et al., 2014), and acid digestion measurement for total Na of the DF core (Sato et al., 2013). For each filter sample, the mass of Na in the terrestrial dust, sea-salt, and mixed particles were calculated as follows:

$$m_{Na} = \frac{W_{Na}}{\sum W_i} \times \frac{\pi {D_{circ}}^3 \rho}{6} \quad (3)$$

where m is mass of Na of the terrestrial dust (m_{nssNa}), ssNa of sea-salt (m_{ssNa1}) or ssNa of mixed particles (m_{ssNa2}), W_{Na} is weight ratio of Na to all elements measured by the EDS, W_i is weight ratio of element i, D_{circ} is particle diameter (defined above), and ρ is particle density. The subscript i refers to all measured elements. The density of terrestrial dust and sea salts were assumed equal (the mean density of crust and that of Na_2SO_4 is ~2.7 g cm^{-3}). The ratio of the mass fraction of ssNa to all Na is written as:

$$\left(\frac{ssNa}{Na}\right)_{subl} = \frac{m_{ssNa1} + m_{ssNa2}}{m_{nssNa} + m_{ssNa1} + m_{ssNa2}} \quad (4)$$

and the result is shown in Fig. 4. Estimated uncertainties for $(ssNa/Na)_{subl}$ were ± ~3 – 8 % based on the EDS measurement error. Also, we assessed the maximum uncertainties associated with the assumptions about the shape and density. For the former, $(ssNa/Na)_{subl}$ under the assumption that all particles are flat are different from those with the spherical assumption by 3 and 8 % for the EDC and DF cores, respectively, on average. For the latter, $(ssNa/Na)_{subl}$ under the assumption that all sea-salt particles are NaCl (2.16 g cm^{-3}) become smaller by 3 and 7% for the EDC and DF cores, respectively, on average.

The values of ssNa from ion measurements was calculated using the following equation:

$$[ssNa^+] = c\,\{[Na^+] - [Ca^{2+}] \cdot (Na^+/Ca^{2+})_{nss}\} \quad (5)$$

$$\text{where } c = \left[1 - \frac{\left(\frac{Na^+}{Ca^{2+}}\right)_{nss}}{\left(\frac{Na^+}{Ca^{2+}}\right)_{ss}}\right]^{-1}. \quad (6)$$

We used published values of $(Na^+/Ca^{2+})_{ss}$ (=23) and $(Na^+/Ca^{2+})_{nss}$ (Bigler et al., 2006). For $(Na^+/Ca^{2+})_{nss}$, we used the value from mean crust (0.56) (Bowen, 1979) and that from high-resolution analysis of the EDC ice core (0.94) (Bigler et al., 2006). The ratios of $ssNa^+$ to Na^+ thus obtained could be expressed as $(ssNa^+/Na^+)_{Bowen}$ and $(ssNa^+/Na^+)_{Bigler}$ for $(Na^+/Ca^{2+})_{nss}$ of 0.56 and 0.94, respectively.

For the DF core, ssNa was also estimated from total Na (tNa) and total Al (tAl) concentrations and the crustal ratio of Na to Al (=0.29) (Sato et al., 2013),

$$[ssNa] = [tNa] - (Na/Al)_{crust} \cdot [tAl]. \quad (7)$$

The $(ssNa/tNa)$ ratio agrees with $(ssNa^+/Na^+)_{Bowen}$ (Fig. 4), which is reasonable because both method use the elemental ratios of mean crust.

The $(ssNa^+/Na^+)_{Bowen}$, $(ssNa^+/Na^+)_{Bigler}$, and *ssNa*/*tNa* ratios can be compared with $(ssNa/Na)_{subl}$ from our data (Fig. 4). The average $(ssNa/Na)_{subl}$ in the EDC core in the LGM, Termination and Holocene agree with both $(ssNa^+/Na^+)_{Bowen}$ and $(ssNa^+/Na^+)_{Bigler}$ within one standard deviation. Closer inspections of the data reveal that the average $(ssNa/Na)_{subl}$ is close to $(ssNa^+/Na^+)_{Bowen}$ and ~10 % higher than $(ssNa^+/Na^+)_{Bigler}$ for the LGM. This seems reasonable because our EDS-based classification may underestimate the terrestrial dust fraction and thus provides the upper bound for the *ssNa*/*Na* ratio.

For the DF core, the average $(ssNa/Na)_{subl}$ for the LGM is similar to $(ssNa^+/Na^+)_{Bowen}$ and ~20% higher than $(ssNa^+/Na^+)_{Bigler}$, possibly suggesting underestimation of the terrestrial fraction of Na in our method. Conversely, the average $(ssNa/Na)_{subl}$ in the Holocene is ~30 and ~20 % lower than the average $(ssNa^+/Na^+)_{Bowen}$ and $(ssNa^+/Na^+)_{Bigler}$, respectively. We note that the standard deviation for the Termination and Holocene $(ssNa/Na)_{subl}$ (11 and 28 %, respectively) is much larger than for the EDC core (4 and 4 %, respectively) due to a few DF samples with extremely low $(ssNa/Na)_{subl}$. Thus, the average value of the 8 Holocene samples might not represent the true average over the period. It should also be noted that the $(ssNa^+/Na^+)_{Bowen}$ and $(ssNa^+/Na^+)_{Bigler}$ of the DF core vary more than those of the EDC core during the Holocene, suggesting that the composition of Na-particles deposited at Dome Fuji has greater variability than those deposited at Dome C.

3.2 Geometric information of particles

The circular equivalent diameter (D_{circ}) and aspect ratio (AR) are shown in Fig. 5 and 6, respectively. In Fig. 5, the full-scales of y-axes are scaled within each type of particles by the ratios of total particle numbers between the LGM, Termination and Holocene to aid visual comparison. The size and AR distributions were fitted with lognormal functions and their modes were calculated (Table 1 and 2).

All the size distributions are unimodal with the modes around 2 μm. In each classification, 68% (1 σ_g) of particles are distributed within a similar range (1.4–1.8 μm). The mode of the terrestrial dust of the EDC core in the LGM, Termination, and Holocene is 1.36, 1.46, and 1.56 μm, respectively. We note that the dust size from the Coulter Counter is larger for the Holocene than for the LGM (Delmonte et al., 2002, 2004a; Lambert et al., 2008), consistent with our result.

The particle sizes are also different between terrestrial dust, sea-salt, and mixed particles. The sea-salt particles are smaller than terrestrial dust particles, although the difference is statistically insignificant for the LGM because of the small number of particles. Note that sea-salt particles in this study are mostly larger than 1 μm, whereas sea-salt aerosols are mainly distributed in sub-μm range

in the troposphere over Antarctic inland (Jourdain et al., 2008; Udisti et al., 2012). Thus, sea-salt particles measured in this study may have coagulated during precipitation and after deposition. As expected, the mixed particles are larger than sea salt and terrestrial dust particles because the mixed particles are produced by collision and coalescence of multiple particles (Fan et al., 1996; Niimura et al., 1998).

The particle sizes in the DF core also show lognormal distributions centered around 2 μm (modal size). The modes of sea-salt particle size are smaller than the dust and mixed particles. However, the mode of dust particle size in the DF core is larger in the LGM than in the Holocene, which is opposite to the result of the EDC core. Also, the modal size of dust in the all period in the DF core are larger than those in the EDC core.

The mode of AR of sea-salt particles is smaller than that of dust and mixed particles both in the EDC and DF cores, suggesting that sea-salt particles are closer to spheres than dust and mixed particles. The mode of AR for terrestrial dust particles is larger in the EDC core than that in the DF core for all the periods, but those for sea salts and mixed particles are similar for the two cores (Table 2).

3.3 Number fractions of terrestrial dust and sea-salt particles

In the EDC core, the fraction of terrestrial dust is the highest in all periods (40 – 64 %, Figs. 7e–g) with large variability (~30 to ~80 %) (Fig. 7a). The sea-salt fraction is very low during the LGM (~5% on average), and it is relatively high from 17 kyr BP until 6 kyr BP (~30% on average, Fig. 7c). The fraction of terrestrial dust is similar for the LGM and Holocene, whereas the sea-salt fraction is ~4 times higher in the Holocene (Fig. 7e and 7g), thus the ratio of sea salts to terrestrial dust is also higher in the Holocene. This is consistent with the ratios of fluxes of insoluble dust and $ssNa^+$ (Wolff et al., 2006; Lambert et al., 2008). We note that, due to potential coagulation of sea-salt particles during precipitation or after deposition, the ratio of number fractions of sea salts and dust from this study may not directly correspond to the ratio of aerosols in the past atmosphere. However, the relative change of the ratio over the deglaciation should reflect the atmospheric change, because the size of sea-salt particles is not significantly different between LGM and Holocene suggesting minor change of the degree of coagulation.

In the DF core, the fraction of sea-salt particles is low in the LGM and it increases after 17 kyr BP, whereas the terrestrial dust fraction is highest in all periods with large scatter and without clear difference between the LGM and Holocene (Figs. 7a, 7h–j). The terrestrial dust fraction is somewhat lower during the Termination. These features are common for the two ice cores. A notable

difference is that the fraction of terrestrial dust in the EDC core is lower than in the DF core for all three periods, as well as for the individual values for almost all data points. Conversely, the average sea-salt fraction is higher in the EDC core than in the DF core for all three periods.

3.4 Composition of Ca-containing particles

The Ca-containing particles are classified as terrestrial dust or mixed particles in this study. Their compositions reflect the original composition at dust sources (e.g. carbonate or gypsum) and the degrees of chemical reactions of calcium carbonate with nitrate or sulfate in the atmosphere, which in turn reflect the transport pathways of terrestrial dust considering the difference in altitudinal distribution of nitrate and sulfate (Legrand et al., 1988; Mahalinganathan and Thamban, 2016). Previous studies based on ion concentrations and Raman spectroscopy have suggested that almost all calcium salt particles found in Antarctic inland cores are calcium sulfate ($CaSO_4$), including gypsum and secondary $CaSO_4$ (by the reaction of $CaCO_3$ with H_2SO_4) (Sakurai et al., 2011; Goto-Azuma et al., 2019). However, we found numerous particles with only a Ca peak (without an S peak) in the EDS measurements. Below, we estimate the chemical composition of calcium salt in our samples.

Particles containing Ca and S (Ca and Cl) are identified to contain $CaSO_4$ ($CaCl_2$), and those containing Ca without any other element are denoted as Ca_{only} particles. In order to avoid uncertainty from Na_2SO_4 in the discussion of Ca-containing particles, we only discuss here the particles containing Ca without Na (Fig. 2). In addition, if atomic ratio $S/Ca = 1$, the Ca containing particles are primary gypsum or fully modified calcium carbonate (by H_2SO_4). The particles with $S/Ca < 1$ are mixture of primary gypsum and calcium carbonate, or partially modified calcium carbonate. Similarly, if $Cl/Ca = 2$, the particles are fully modified calcium carbonate (by HCl), and if $Cl/Ca < 2$, they are interpreted as partially modified. If all Ca, S and Cl are detected in a particle, it is interpreted to contain both $CaSO_4$ and $CaCl_2$.

In the EDC core, the Ca-containing particles are dominated by $CaSO_4$ (80%) in the LGM (Fig. 8a). After ~17 kyr BP, Ca_{only} becomes dominant (62%) and the number fraction of particles with $S/Ca < 1$ also increased (Fig. 8a). Therefore, our data indicate significant contribution of non-$CaSO_4$ calcium salt during the Termination and Holocene, despite high availability of H_2SO_4. The $CaCl_2$ particles rarely present without discernible trend.

In the DF core, particles containing $CaSO_4$ are also dominant (82%) during the LGM, and the Ca_{only} fraction increases thereafter (Fig. 8b). However, unlike in the EDC core, about half of the particles containing $CaSO_4$ show $S/Ca < 1$ during the LGM. Moreover, the average fraction of Ca_{only}

particles during the Termination to Holocene is smaller than in the EDC core, while the fraction of $CaCl_2$ is higher than in the EDC core throughout the entire period.

3.5 Compositions of sea-salt particles

The fractions of the atomic ratios of Na, S, and Cl in individual particles are plotted on ternary diagrams to investigate sea-salt modification during the LGM and Holocene (Fig. 9). To exclude uncertainty from nssNa, we only analyzed sea-salt particles without dust components (Si, Al, and Ca). In the EDC core, few data are close to the initial sea-salt ratio, indicating that most of initial sea-salt particles are modified in both the LGM and Holocene (Fig. 9a and 9b). Most particles are distributed along the line with S = 0 or the line with Cl = 0 for both the LGM and Holocene, indicating that all Cl is lost from sea-salt particles if they react with H_2SO_4 or MSA. On the other hand, Cl loss is incomplete if sea-salt particles react with HNO_3 (data along the S = 0 line). Comparison of the LGM and Holocene data reveals that the range of Cl loss by HNO_3 (the spread of data along the S = 0 line) is similar for the two periods. Overall, 93 % (98 %) of initial sea-salt particles in the EDC core during the LGM (Holocene) are partially or fully modified by HNO_3, H_2SO_4, or MSA. Among the fully modified sea-salt particles, approximately 24% (13%) are modified by HNO_3 and ~89% (~96%) are modified by H_2SO_4 or MSA in the LGM (Holocene) (the addition of the two values exceeds 100 % because some particles are modified by both acids). Among the particles modified by H_2SO_4 or MSA (along the Cl = 0 line), modification by MSA is more significant in the Holocene than in the LGM.

The modification of sea-salt particles is less severe in the DF core both in the LGM and Holocene (Fig. 9c and 9d). For the LGM, many data points are close to the initial sea-salt composition and there are few data with Cl ≈ 0, indicating that many of initial sea-salt particles are modified only slightly. For the Holocene, the magnitude of Cl loss by HNO_3 is more variable (i.e., data along the line with S = 0 are distributed over a much wider range) than in the LGM. Approximately 58% (85%) of initial sea-salt particles are modified partially or fully during the LGM (Holocene). Approximately 24% (30%) of them are modified by HNO_3 and ~52% (~79%) are modified by H_2SO_4 or MSA in the LGM (Holocene). The DF data also show that the fraction of sea-salt particles modified by H_2SO_4 and MSA is larger in the Holocene than in the LGM.

To investigate the temporal changes in Cl depletion from the sea-salt particles from the LGM to early Holocene and their difference between the EDC and DF cores, we plot the fraction of atomic ratio of Cl in the sum of Na, S, and Cl in individual sea-salt particles (initial and modified) against the age of ice (Fig. 10). The area of markers (open circles) on the zero line is proportional to

480 the fraction of fully modified sea-salt particles (i.e. sea-salt particles with Cl = 0). The black and blue
481 dashed lines indicate the Cl fractions for initial sea salts from seawater and sea ice, respectively, with
482 the uncertainty range depicted by gray shading.

483 For the EDC core, most data points are distributed less than 50 %, and most of them are
484 fully modified. Only a small number of particles are unmodified. No discernable trend is observable
485 for the distribution of the data of partially modified sea-salt particles (small dots above 0%) from the
486 LGM to Holocene. On the other hand, fully modified particles are more abundant after 18 kyr BP
487 than they are before.

488 The DF data have similarity with the EDC data in that fully modified sea-salt particles are
489 more abundant after 18 kyr BP. However, close inspection of the data reveals that the fraction of
490 fully modified particles is sometimes small during the Termination and Holocene in the DF core,
491 which is not the case for the EDC core (most are above > 90 %). The particles having the Cl fraction
492 of initial sea salts are more abundant throughout the studied period in the DF core. Few data points
493 are below 40 % before 18 kyr BP in the DF core, while the most data points are below that level in
494 the EDC core.

495

496 **4 Discussion**

497 **4.1 Dust fluxes in the EDC and DF cores**

498 The number fraction of terrestrial dust in the EDC core is lower than in the DF core during
499 all climate periods (Fig. 7). We first consider the uncertainties in the classification scheme to
500 examine the robustness of this result. As discussed in Section 3.1, for both the EDC and DF cores,
501 our particle classification probably underestimates the number fraction of terrestrial dust particles
502 containing Na, especially in the LGM, while it overestimates the fraction of terrestrial dust particles
503 containing Ca in the Holocene. It can be seen from Fig. 4 that the $(ssNa^+/Na^+)_{Bowen}$ ratio is higher
504 than $(ssNa^+/Na^+)_{Bigler}$ by ~10 and ~20 % for the EDC and DF cores, respectively (where
505 $(nssNa^+/nssCa^{2+})_{Bigler} = 0.94$ is assumed) (Bigler et al., 2006). The larger discrepancy for the DF core
506 suggests a more pronounced underestimation of the terrestrial dust fraction associated with nssNa.
507 Regarding the Ca-containing particles, ion concentration analyses suggest that $ssCa^{2+}/Ca^{2+}$ in the
508 EDC core (Bigler et al., 2006) is higher than in the DF core (Oyabu et al., 2014). Thus, the
509 misclassification of ssCa particles into terrestrial dust is probably more significant for the EDC core
510 than for the DF core. We also consider the possible misclassification of terrestrial Fe-containing
511 particles into “others/unknown.” However, as they comprise only 0.5 % of all particles, the possible
512 misclassification of Fe-containing particles is not a significant source of error. Therefore, although

513 quantitative estimations of the above errors are difficult, the misclassifications do not affect the
514 overall finding that the number fraction of terrestrial dust is lower in the EDC core than in the DF
515 core.

516 The lower dust fraction in the EDC core does not necessarily indicate lower dust flux at the
517 Dome C site. In the following, we explore the possibility of comparing dust number concentrations
518 between the EDC and DF cores by combining our sublimation-EDS results with ion concentration
519 data. We compare the fluxes of $ssNa^+$ (from ion analyses) and sizes of ssNa particles (from
520 sublimation-EDS) between the two cores, which are the basis for the comparison of dust
521 concentrations. The average $ssNa^+_{Bowen}$ fluxes for the EDC core are in accord with those of the DF
522 core to within 8% in the LGM and Termination (Table 3, Fig. 11a). In the Holocene, the average
523 $ssNa^+$ fluxes in the EDC core are lower than in the DF core because of a small number of high values
524 in the DF data (possibly related to outlier rejection in the published EDC dataset; all the measured
525 data are included in the DF dataset), but the background values are similar. The EDS-derived
526 elemental mass ratios of individual particles, together with the particle classifications, can also be
527 used to divide Na^+ fluxes into sea-salt and non-sea-salt components ($ssNa^+_{subl}$ and $nssNa^+_{subl}$), which
528 are independent of those estimated by the combination of Na^+ and Ca^{2+}. The $ssNa^+_{subl}$ and $nssNa^+_{subl}$
529 are derived with following equation, $ssNa^+_{subl} = \left(\frac{ssNa}{Na}\right)_{subl} \times Na^+$, and (8)

530 $$nssNa^+_{subl} = \left(\frac{nssNa}{Na}\right)_{subl} \times Na^+. \quad (9)$$

531 $(ssNa/Na)_{subl}$ and $(nssNa/Na)_{subl}$ are derived from the equation (4) in the Section 3.1. The $ssNa^+_{subl}$
532 and $nssNa^+_{subl}$ fluxes in the EDC and DF cores agree with the $ssNa^+_{Bowen}$ and $nssNa^+_{Bowen}$ fluxes,
533 respectively albeit with somewhat larger scatter (Fig. 11a and 11b). For the following discussion, we
534 assume that each mixed particle consists of one sea-salt particle and one terrestrial dust particle and
535 the average number concentrations of sea-salt particles are equal for the two cores in each period.
536 Given these assumptions and the particle number fractions of terrestrial dust (N_{dust}), sea-salt (N_{ss}),
537 and mixed particles (N_{mix}) (Fig. 7), the number concentrations ratios of soluble and insoluble dust
538 particles (including those attached to sea salts) between the EDC and DF cores ($NCR_{DF/EDC}$) are
539 obtained from:

540 $$NCR_{DF/EDC} = \frac{(N_{EDC,ss} + N_{EDC,mix})}{(N_{DF,ss} + N_{DF,mix})} \times \frac{(N_{DF,dust} + N_{DF,mix})}{(N_{EDC,dust} + N_{EDC,mix})}. \quad (10)$$

541 The resulting $NCR_{DF/EDC}$ = 1.5, 1.5 and 1.6 for the LGM, Termination, and Holocene, respectively.

The modal sizes of dust in the DF core are larger than in the EDC core by a factor of 1.1–1.4, thus the dust mass fluxes may be significantly higher in the DF core than in the EDC core. With our size data, we can roughly estimate the mass fluxes ratios of dust (including those attached to sea salts) between the two cores ($MFR_{DF/EDC}$) by weighting the ratios of the number concentrations (as given above) with the ratios of modal volume of dust and sea-salt particles in the DF and EDC cores ($MVR_{DF/EDC,dust}$ and $MVR_{DF/EDC,ss}$).

$$MFR_{DF/EDC} = NCR_{DF/EDC} \times \frac{MVR_{DF/EDC,dust}}{MVR_{DF/EDC,ss}} \quad (11)$$

The $MFR_{DF/EDC}$ thus deduced are 3, 2 and 3 for the LGM, Termination and Holocene, respectively, suggesting that dust flux at Dome Fuji was higher than at Dome C in all studied periods. These ratios are inconsistent with those using published data of insoluble dust measured by different laboratories (Lambert et al., 2008; Dome Fuji Ice Core Project Members, 2017), which show higher dust flux at Dome C. On the other hand, our results are consistent with those from numerical modeling studies of dust transport and deposition, which simulated dust flux (or concentration) in the Dome Fuji region that are ~2 times higher than in the Dome C region in both the Holocene and LGM (Albani et al., 2012; Ohgaito et al., 2018). Fig. 12 shows re-analyzed model results of Ohgaito et al. (2018), focused on Antarctica at the highest available resolution. According to the analyses, the dust deposition flux at Dome Fuji at 21 kyr BP is estimated to be 1.6 times higher than at Dome C, which is qualitatively consistent with our estimation for the LGM (i.e., 3 times higher). The simulation suggests the importance of glaciogenic Patagonian dust in the LGM through sensitivity experiments with and without Patagonian dust flux (Ohgaito et al, 2018). The spatial gradient of dust deposition over Antarctica, including higher values at Dome Fuji than at Dome C, is linked to large-scale dust transport pattern (Fig. 12), which clearly shows decreasing deposition flux on the leeward of Patagonia with increasing transport distance. The smaller DF/EDC deposition flux ratio in the model result than in the ice-core data may be reasonable, because numerical models are expected to produce smoother spatial pattern than reality due to a phenomenon called numerical diffusion.

For the LGM, the mode of AR for dust in the EDC core (1.42) are slightly higher than that in the DF core (1.38) (Table 2), which may be significant considering that the mode of AR for Holocene sea salts are the same for the two cores to the last digit (reasonable for abundant non-mineral particles). Also, the mode of circular equivalent diameter of dust in the EDC core (1.36 μm) is significantly smaller than in the DF core (1.94 μm). These results suggest that dust particles transported to Dome C region are more elliptic and smaller on average than those at Dome Fuji, which may be due to longer transport of dust reaching Dome C than Dome Fuji from the dominant glaciogenic dust source in Patagonia. During atmospheric transport, dust particles with higher AR

575 may become more abundant with increasing transport distance, as inferred from much slower settling
576 velocity of mineral particles than that of spheres of equivalent volumes (Cui et al., 1983; Pye, 1994).
577 Longer transport pathway of Patagonian dust to Dome C than to Dome Fuji has also been
578 demonstrated by an atmospheric trajectory model, albeit for modern climate (Sudarchikova et al.,
579 2015). Another important observation from our data is that the modal dust size in the EDC core
580 shifted to a larger value (from 1.36 to 1.56 μm) from the LGM to Holocene, while the sign of change
581 is opposite in the DF core (from 1.94 to 1.70 μm). The dust model of Albani et al. (2012) produced
582 qualitatively consistent result for the EDC core (suggesting enhanced en route wet removal in the
583 Holocene), but inconsistent result for the DF core. Possible explanations for the larger dust in the
584 LGM DF ice may be enhanced meridional transport (shorter pathways) of Patagonian dust to Dome
585 Fuji (Delmonte et al., 2004a) and/or enhanced dry deposition at the site (Albani et al., 2012).

586

587 **4.2 Change in composition of calcic dust**

588 As described in Section 3.4, most Ca containing particles contains $CaSO_4$ during the LGM,
589 but its fraction decreases and the fraction of Ca_{only} ($CaCO_3$ and/or $Ca(NO_3)_2$) increases after 17 kyr
590 BP in both the EDC and DF cores (Fig. 8). These fractional changes may reflect changes in dust
591 sources and transport processes.

592 We first discuss chemical forms of the Ca_{only} particles after 17 kyr BP. We speculate that
593 they are mostly $Ca(NO_3)_2$ because $CaCO_3$ is highly reactive with HNO_3 (Usher et al., 2003) and
594 NO_3^- and Ca^{2+} concentrations in both cores are highly correlated (Röthlisberger et al., 2000, 2002;
595 Watanabe et al., 2003a; Iizuka et al., 2008). Studies of modern surface snow from coastal to
596 high-elevation sites in Antarctica (including Dome C) indeed suggest that $Ca(NO_3)_2$ forms during
597 long-range transport of calcic dust (Udisti et al., 2004; Mahalinganathan and Thamban, 2016).
598 Delmonte et al. (2017) found $CaCO_3$ particles (calcite and aragonite) and diatom valves in the LGM
599 section of the Dome B core and proposed that their source was exposed Patagonian continental shelf.
600 The supply of such $CaCO_3$ should decrease with rising sea level, thus it is unlikely to be the major
601 component of Ca_{only} particles after 17 kyr BP, whose fraction increases with time. Another possible
602 component of Ca_{only} is $CaCO_3$ from sea-ice surface (ikaite and calcium carbonate monohydrate),
603 which has been found in the Talos Dome (a coastal dome) firn core (Sala et al., 2008). However,
604 considering the large fractions of modified sea-salt particles during the Termination and Holocene in
605 the EDC and DF cores, we speculate that $CaCO_3$, which is more reactive than NaCl, from the sea-ice
606 surface is unlikely to be abundant in the Antarctic interior. Even if such $CaCO_3$ were present in the

EDC and DF cores, its abundance should decrease with decreasing sea-salt concentrations during the Termination, which is again contradictory to our data.

If $CaSO_4$ and $Ca(NO_3)_2$ found in Antarctic snow and ice are mainly produced by atmospheric reaction of $CaCO_3$ with H_2SO_4 and HNO_3, respectively (Legrand & Mayewski, 1997; Gibson et al., 2006), such reactions may occur at different altitudes (Legrand et al., 1988; Mahalinganathan & Thamban, 2016). The principal source of atmospheric H_2SO_4 is photochemical oxidation of dimethyl sulfide emitted by marine biological activity (Davis et al., 1998), whereas HNO_3 is formed from nitrogen oxides mostly in the mid- to upper troposphere and stratosphere (Wolff, 1995; Savarino et al., 2007). Therefore, the fractions of $CaSO_4$ and $Ca(NO_3)_2$ particles may reflect the altitude of atmospheric transport of dust particles (marine boundary layer for $CaSO_4$ and free troposphere for $Ca(NO_3)_2$).

Previous studies on the mineralogy of EDC dust have identified that the dominant dust source area was Patagonia during the LGM and that multiple dust sources including Australia may have contributed after ~16 kyr BP (Delmonte et al., 2004b, 2008; Revel-Rolland et al., 2006; Siggaard-Andersen et al., 2007; Marino et al., 2008; Vallelonga et al., 2010; Wegner et al., 2012; Gili et al., 2016). Atmospheric model simulations have suggested that Patagonian dust is transported via the lower troposphere, while Australian dust is transported via the mid- to upper troposphere (Li et al., 2008; Krinner et al., 2010). Our results of the dominance of $CaSO_4$ in the LGM and increased Ca_{only} in the Termination and Holocene are thus consistent with the dominant dust contribution from Patagonian during the LGM and the hypothesis of increased Australian dust contribution during the Termination and Holocene. $CaSO_4$ particles would partly originate in sea salt from open ocean or sea ice (Section 3.1). The contribution of ocean-origin $CaSO_4$ is smaller (< 10 %) in the LGM than in the early Holocene (about 50 %) from ion concentrations, thus it does not affect the above conclusion.

A recent work proposed that $CaSO_4$ in glacial periods may largely originate from primary gypsum (Goto-Azuma et al., 2019). If this was the case, our data is still consistent with the dominant Patagonian dust source during the LGM because the sources of gypsum lie in Patagonia (Drewry et al., 1974; Nickovic et al., 2012). Comparison of our EDC and DF data for the LGM reveals that the DF core contains abundant particles with $Ca/S < 1$ (comparable to the particles with $Ca/S = 1$), while the EDC core contains few particles with $Ca/S < 1$. Considering the longer distance from Patagonia to EDC than to DF, our data may suggest major contribution of $CaSO_4$ derived from the reaction of $CaCO_3$ and H_2SO_4. We note that our data do not necessarily contradict with the conclusion of Goto-Azuma et al. (2019) that biogenic sulfur emission was reduced in glacial periods, because the conclusion holds with large range of proportion of primary gypsum to total $CaSO_4$.

640 The fraction of $CaSO_4$ is higher in the DF core than in the EDC core after ~17 kyr BP,
641 suggesting continuation of major Patagonian dust contribution to Dome Fuji region after 17 kyr BP.
642 This is qualitatively consistent with the results of modern trajectory analyses (Neff & Bertler, 2015),
643 which have shown that the Dome Fuji site receives a higher proportion of Patagonian dust than the
644 Dome C site.

645

646 **4.3 Modifications of sea-salt particles**

647 Our results show that most initial sea-salt particles (NaCl) react with HNO_3, H_2SO_4, or
648 MSA in the atmosphere before reaching Dome C, or in snow after deposition in both the LGM and
649 Holocene (Figs. 9 and 10). The DF core shows a higher fraction of modified sea-salt particles in the
650 Termination and Holocene than in the LGM (Figs. 9 and 10). The results from the two ice cores are
651 thus consistent in terms of the high fraction of modified sea-salt particles in the Holocene.

652 The preservation of Cl^- from initial sea-salt particles may be estimated by comparing the
653 Cl^-/Na^+ ratio of ice cores with the sea-water ratio of 1.8 (e.g., Röthlisberger et al., 2003). The Cl^-/Na^+
654 ratio in the LGM is 1.65 and 1.70 for the EDC and DF cores, respectively (Littot et al., 2002; Wolff
655 et al., 2006; Oyabu et al., 2014; Goto-Azuma et al., 2019), suggesting > 90 % preservation. Recently,
656 Legrand et al. (2017) proposed higher Cl^-/Na^+ ratio in mobile sea-salt aerosols in the LGM of up to
657 2.2 through the precipitation of mirabilite ($Na_2SO_4 \cdot 10H_2O$) on expanded sea-ice surface. If we take
658 2.0 as the initial Cl^-/Na^+ ratio, the same ion data suggest ~82 and ~85 % preservation for the EDC
659 and DF cores, respectively. For the Holocene ice (Röthlisberger et al., 2003; Oyabu et al., 2014;
660 Goto-Azuma et al., 2019), the estimated Cl^- preservation rates are ~28% and ~100% for the EDC and
661 DF cores, respectively (Cl^-/Na^+ = ~0.5 and ~2, respectively).

662 From this study, the number fractions of unmodified sea-salt particles (i.e. those within the
663 gray band in Fig. 10a) in all sea-salt particles are 7 and 1 % in the LGM and in the Holocene,
664 respectively, in the EDC core. These values are strikingly lower than the ion-based Cl^- preservation
665 rate described above. The DF core shows higher rates of Cl^- preservation (42 % in the LGM, 15 % in
666 the Holocene) than the EDC core, but they are also much lower than the ion-based Cl^- preservation
667 rate.

668 The large discrepancies between the Cl^- preservation rates from the sublimation-EDS and
669 ion measurements indicate the existence of major non-NaCl substance in the ice sheet that include
670 Cl^-. Here, non-NaCl chloride salts are unlikely to be the major source of Cl^- because such particles
671 comprise only 1% of all particles that we studied here. Therefore, most Cl^- should be present as HCl
672 in the ice. Laboratory experiments have suggested that gaseous HCl may be incorporated in ice as

673 solid solution, aqueous solution, or HCl hexahydrate, and that HCl inclusion could occur during
674 aerosol transport and snow crystal formation in the atmosphere, as well as after aerosol deposition
675 during snow metamorphism (Domine and Thibert, 1995a, b; Thibert and Domine, 1997).

676 A striking difference between the data from the two cores is that the sea-salt particles in
677 the DF core are modified much less than those in the EDC core in both the LGM and Holocene (Figs.
678 9 and 10). For the Holocene, the sum of acid concentrations ($[SO_4^{2-}] + [NO_3^-]$) is much higher than
679 the sum of sea-salt and dust concentrations ($[Na^+] + [Ca^{2+}] + [Mg^{2+}]$) in both the EDC and DF cores
680 (Table 4). For the LGM, the sum of acid concentrations is lower than the sum of sea-salt and dust
681 concentrations, and the magnitude of the imbalance is similar in the two cores. Thus, simple
682 consideration of the ionic balance predicts similar rates of sea-salt modification for the two cores,
683 which clearly contradicts the sublimation-EDS data. We suggest that the primary cause for the larger
684 rate of unmodified sea-salt particles in the DF core is the high concentration of terrestrial dust, which
685 reduces the acids available for sea-salt modification.

686 The larger NaCl fraction in the DF core in comparison with the EDC core would not fully
687 explain the much larger Cl^-/Na^+ ratio in the DF core in the Holocene. This suggests that most Cl^- was
688 lost to the atmosphere from the snow at Dome C, while it was preserved at Dome Fuji as NaCl and
689 solid solution. The significant difference in Cl^- preservation might be attributable to post-deposition
690 snow redistribution and near-surface environmental properties (such as ventilation and light), which
691 might affect the likelihood and magnitude of the reactions between sea salt and acids, and the rate of
692 evaporation of HCl produced in snow. To clarify the causes of the higher modification rate of
693 sea-salt particles as well as the greater Cl^- loss in the EDC core in comparison with the DF core,
694 year-round observations of atmospheric aerosols and their deposition at the studied sites are
695 desirable.

696

697 **5 Conclusions**

698 We measured the elemental compositions and size distributions of dust and sea-salt
699 particles in the EDC core from the LGM to early Holocene (26–7 kyr BP), and compared them with
700 the data from the DF core measured using the same method. The method extracts nonvolatile
701 particles from ice samples by sublimating ice and volatile materials, which are measured using
702 SEM-EDS. The main findings are summarized as follows.

703 The sea-salt fluxes are approximately the same for both cores, whereas the dust flux in the
704 EDC core is 2 – 3 times lower than in the DF core from the LGM to the Holocene. The significantly
705 lower dust flux at Dome C during the LGM is consistent with model results of dust transport from

706 Patagonian glaciogenic dust source and deposition on those sites (Albani et al., 2012; Ohgaito et al.,
707 2018). The smaller modal size and larger aspect ratio of dust particles in the EDC core support the
708 dominance of Patagonian source. The high fractions of $CaSO_4$ in both cores during the LGM suggest
709 that most dust particles were transported via the lower troposphere. During the Termination and early
710 Holocene, the fraction of $Ca(NO_3)_2$ increases especially in the EDC core, which is consistent with
711 the hypothesis that multiple dust sources including Australia contributed to the dust flux to the Dome
712 C region. For the Dome Fuji region, the Patagonian source possibly continued to dominate the dust
713 supply. The modal dust size shifted to a larger (smaller) value in the EDC (DF) core from the LGM
714 to Holocene, which should reflect changes in dust source, transport pathways and en route removal
715 processes.

716 In the DF core, NaCl particles were found more abundant than in the EDC core in both the
717 LGM and Holocene. A possible cause for this difference may be the higher concentration of
718 terrestrial dust in the DF core, reducing acids to react with sea salts. However, the high NaCl fraction
719 in the DF core is still insufficient to explain the very large Cl^-/Na^+ ratio (higher than seawater ratio)
720 in the early Holocene, suggesting Cl^- preservation at Dome Fuji as both NaCl and solid solution,
721 while most Cl^- was lost to the atmosphere from snow at Dome C. The significant difference in Cl^-
722 preservation might be related to post-depositional snow redistribution and near-surface
723 environmental properties. Modern observations of aerosol transport and deposition at the studied
724 sites could help improve the understanding of the processes of sea-salt modification and Cl^- loss in
725 Antarctic inland regions.

726

727 **Appendix**

728 **Figure A1.** Atomic fractions of Ti, Fe, Al, Si, Na, Mg, K, Ca, S, and Cl of all the particles in the
729 EDC core measured using SEM-EDS. δD is derived from Jouzel et al. (2007). Vertical lines in the
730 figure of δD indicate measured sample age.

731 **Figure A2.** Same as Fig. A1 but for the DF core. $\delta^{18}O$ is derived from Dome Fuji Ice Core Project
732 Members (2017).

733

734 **Acknowledgments**

735 We thank the logistics and drilling teams responsible for the recovery of the Dome C ice core. This
736 work is a contribution to EPICA, a joint European Science Foundation/European Commission (EC)
737 scientific program, funded by the EC (EPICA-MIS) and by national contributions from Belgium,

Denmark, France, Germany, Italy, The Netherlands, Norway, Sweden, Switzerland, and the UK. We are grateful to T. Karlin of Stockholm University for helping us set up the sublimation system at Stockholm University, G. Teste of Institut des Géosciences de l'Environnement (IGE) for preparing ice samples, M. Furusaki of ILTS for help with the SEM-EDS analysis, T. Ishiwa of NIPR for help to draw a map of Antarctica, and R. Udisti of the University of Florence, B. Delmonte of the University of Milano-Bicocca, M. Legrand of IGE, and T. Uchida of Hokkaido University for valuable comments and discussion. This study was supported by the Nordic Centre of Excellence Cryosphere-atmosphere interactions in a changing Arctic climate (CRAICC) (to I.O.), by JSPS KAKENHI Grant Numbers 40370043, 26257201, 26610147 (to Y.I.), 17K12816, 17J00769 (to I.O.), 15KK0027, 17H06320 (to K.K.), 17H06104 and 17H06323 (to A.A-O.), and by the Grant for Joint Research Program of ILTS, Hokkaido University (to Y.I.). I.O. and Y.I. were supported by the JSPS Institutional Program for Young Researcher Overseas Visits. E.W. is funded by the Royal Society. The model experiments are supported by the Integrated Research Program for Advancing Climate Models (TOUGOU programme) from the Ministry of Education, Culture, Sports, Science and Technology (MEXT), Japan and conducted on the Earth Simulator of JAMSTEC. The comments from three reviewers greatly helped improve the manuscript. The authors declare that they have no conflict of interest. Data on nonvolatile particles of the EDC and DF cores and ion concentrations of the DF core are available at the NIPR ADS data repository (https://ads.nipr.ac.jp/dataset/A20191212-001; for inquiry: oyabu.ikumi@nipr.ac.jp).

References

Albani, S., N. M. Mahowald, B. Delmonte, V. Maggi, and G. Winckler (2012), Comparing modeled and observed changes in mineral dust transport and deposition to Antarctica between the Last Glacial Maximum and current climates, *Clim. Dynam.*, *38*(9–10), 1731–1755, doi:10.1007/s00382-011-1139-5.

Basile, I., F. E. Grousset, M. Revel, J. R. Petit, P. E. Biscaye, and N. I. Barkov (1997), Patagonian origin of glacial dust deposited in East Antarctica (Vostok and Dome C) during glacial stages 2, 4 and 6, *Earth Planet. Sci. Lett.*, *146*(3–4), 573–589, doi:10.1016/S0012-821X(96)00255-5.

Bigler, M., A. Svensson, E. Kettner, P. Vallelonga, M. E. Nielsen, and J. P. Steffensen (2011), Optimization of high-resolution continuous flow analysis for transient climate signals in ice cores, *Environ. Sci. Technol.*, *45*(10), 4483–4489, doi:10.1021/es200118j.

Bigler, M., R. Röthlisberger, F. Lambert, T. F. Stocker, and D. Wagenbach (2006), Aerosol deposited in East Antarctica over the last glacial cycle: Detailed apportionment of continental and sea-salt contributions, *J. Geophys. Res. Atmos.*, *111*(D), D08205, doi:10.1029/2005JD006469.

Bowen, H. J. M. (1979), *Environmental Chemistry of the Elements* (Academic Press, London).

Cui, B., P. D. Komar and J. Baba (1983), Settling Velocities of Natural Sand Grains in Air, *J. Sediment. Res., 5 (43)*, 1205-1211, doi: 10.1306/212F8346-2B24-11D7-8648000102C1865D.

Davis, D., G. Chen, P. Kasibhatla, A. Jefferson, D. Tanner, F. Eisele, D. Lenschow, W. Neff, and H. Berresheim (1998), DMS oxidation in the Antarctic marine boundary layer: Comparison of model simulations and field observations of DMS, DMSO, $DMSO_2$, H_2SO_4(g), MSA(g), and MSA(p), *J. Geophys. Res.*, *103*(D), 1657–1678, doi:10.1029/97JD03452.

Delmonte, B., et al. (2017), Causes of dust size variability in central East Antarctica (Dome B): Atmospheric transport from expanded South American sources during Marine Isotope Stage 2, *Quat. Sci. Rev.*, *168*, 55–68, doi:10.1016/j.quascirev.2017.05.009.

Delmonte, B., J. Petit, and V. Maggi (2002), Glacial to Holocene implications of the new 27000-year dust record from the EPICA Dome C (East Antarctica) ice core, *Clim. Dynam.*, *18*(8), 647–660, doi:10.1007/s00382-001-0193-9.

Delmonte, B., J. R. Petit, K. K. Andersen, I. Basile-Doelsch, V. Maggi, and V. Y. Lipenkov (2004a), Dust size evidence for opposite regional atmospheric circulation changes over east Antarctica during the last climatic transition, *Clim. Dynam.*, *23*(3–4), 427–438, doi:10.1007/s00382-004-0450-9.

Delmonte, B., I. Basile-Doelsch, J. R. Petit, V. Maggi, M. Revel-Rolland, A. Michard, E. Jagoutz, and F. Grousset (2004b), Comparing the EPICA and Vostok dust records during the last 220,000

790 years: stratigraphical correlation and provenance in glacial periods, *Earth Sci. Rev.*, *66*(1), 63–87,
791 doi:10.1016/j.earscirev.2003.10.004.
792 Delmonte, B., P. S. Andersson, M. Hansson, H. Schöberg, J. R. Petit, I. Basile-Doelsch, and V.
793 Maggi (2008), Aeolian dust in East Antarctica (EPICA-Dome C and Vostok): Provenance during
794 glacial ages over the last 800 kyr, *Geophys. Res. Lett.*, *35*(7), L07703,
795 doi:10.1029/2008GL033382.
796 Dome Fuji Ice Core Project Members (2017), State dependence of climatic instability over the past
797 720,000 years from Antarctic ice cores and climate modeling, *Sci Adv.*, *3*(2), e1600446,
798 doi:10.1126/sciadv.1600446.
799 Domine, F., and E. Thibert (1995a), Relationship between atmospheric composition and snow
800 composition for HCl and HNO_3, in: Biogeochemistry of seasonally snow-covered catchments,
801 paper presented at Proceedings of a Boulder Symposium, IAHS.
802 Domine, F., and E. Thibert (1995b), Determining past atmospheric HCl mixing ratios from ice core
803 analyses, *J. Atmos. Chem.*, *21*(2), 165–186, doi:10.1007/BF00696579.
804 Drewry, G. E., A. T. S. Ramsay, and A. G. Smith (1974), Climatically Controlled Sediments, the
805 Geomagnetic Field, and Trade Wind Belts in Phanerozoic Time, *J. Geol.*, 82(5), 531–553,
806 doi:10.1086/628005
807 EPICA Community Members (2004), Eight glacial cycles from an Antarctic ice core, *Nature*, *429*,
808 623–628, doi:10.1038/nature02599.
809 Fan, X. B., K. Okada, N. Niimura, K. Kai, K. Arao, G. Y. Shi, Y. Qin, and Y. Mitsuta (1996), Mineral
810 particles collected in China and Japan during the same Asian dust-storm event, *Atmos. Environ.*,
811 *30*(2), 347–351, doi:doi/10.1016/1352-2310(95)00271-Y.
812 Fischer, H., et al. (2007), Reconstruction of millennial changes in dust emission, transport and
813 regional sea ice coverage using the deep EPICA ice cores from the Atlantic and Indian Ocean
814 sector of Antarctica, *Earth Planet. Sci. Lett.*, *260*(1), 340–354, doi:10.1016/j.epsl.2007.06.014.
815 Fischer, H., H. Traufetter, R. Oerter, R. Weller, and H. Miller (2004), Prevalence of the Antarctic
816 Circumpolar Wave over the last two millennia recorded in Dronning Maud Land ice, *Geophys.*
817 *Res. Lett.*, *31*(L08202), doi:10.1029/2003GL019186.
818 Fujita, S., F. Parrenin, M. Severi, H. Motoyama, and E. Wolff (2015), Volcanic synchronization of
819 Dome Fuji and Dome C Antarctic deep ice cores over the past 216 kyr, *Clim. Past*, *11*, 1395–1416,
820 doi:10.5194/cp-11-1395-2015.
821 Geilfus, N. X., R. J. Galley, M. Cooper, N. Halden, A. Hare, F. Wang, D. H. Søgaard, and S.
822 Rysgaard (2013), Gypsum crystals observed in experimental and natural sea ice, *Geophys. Res.*
823 *Lett.*, *40*(24), 6362–6367, doi:10.1002/2013GL058479.

824 Gibson, E. R., P. K. Hudson, and V. H. Grassian (2006), Aerosol chemistry and climate: Laboratory
825 studies of the carbonate component of mineral dust and its reaction products, *Geophys. Res. Lett.*,
826 *33*(13), 1266–1265, doi:10.1029/2006GL026386.
827 Gili, S., D. M. Gaiero, S. L. Goldstein, F. Chemale Jr, E. Koester, J. Jweda, P. Vallelonga, and M. R.
828 Kaplan (2016), Provenance of dust to Antarctica: A lead isotopic perspective, *Geophys. Res. Lett.*,
829 *43*, 2291–2298, doi:10.1002/ 2016GL068244.
830 Goto-Azuma, K., et al. (2019), Reduced marine phytoplankton sulphur emissions in the Southern
831 Ocean during the past seven glacials, *Nat. Commun.*, *10*, 1–7, doi: 10.1038/s41467-019-11128-6.
832 Grousset, F. E., P. E. Biscaye, M. Revel, J. R. Petit, K. Pye, S. Joussaume, and J. Jouzel (1992),
833 Antarctic (Dome C) ice-core dust at 18 k.y. B.P. - Isotopic constraints on origins, *Earth Planet.*
834 *Sci. Lett.*, *111*(1), 175–182, doi:10.1016/0012-821X(92)90177-W.
835 Hara, K., K. Osada, M. Kido, M. Hayashi, K. Matsunaga, Y. Iwasaka, T. Yamanouchi, G. Hashida,
836 and T. Fukatsu (2004), Chemistry of sea-salt particles and inorganic halogen species in Antarctic
837 regions: Compositional differences between coastal and inland stations, *J. Geophys. Res.*,
838 *109*(D20208), doi:10.1029/2004JD004713.
839 Hara, K., S. Matoba, M. Hirabayashi, and T. Yamasaki (2017), Frost flowers and sea-salt aerosols
840 over seasonal sea-ice areas in northwestern Greenland during winter–spring, *Atmos. Chem. Phys.*,
841 *17*(13), 8577–8598, doi:10.5194/acp-17-8577-2017.
842 Iizuka, Y., A. Tsuchimoto, Y. Hoshina, T. Sakurai, M. Hansson, T. Karlin, K. Fujita, F. Nakazawa, H.
843 Motoyama, and S. Fujita (2012b), The rates of sea salt sulfatization in the atmosphere and surface
844 snow of inland Antarctica, *J. Geophys. Res.*, *117*, D04308, doi:10.1029/2011JD016378.
845 Iizuka, Y., B. Delmonte, I. Oyabu, T. Karlin, and V. Maggi (2013), Sulphate and chloride aerosols
846 during Holocene and last glacial periods preserved in the Talos Dome Ice Core, a peripheral
847 region of Antarctica, *Tellus B*, *65*(20197), 1–9, doi:10.3402/tellusb.v65i0.20197.
848 Iizuka, Y., H. Ohno, R. Uemura, T. Suzuki, I. Oyabu, Y. Hoshina, K. Fukui, M. Hirabayashi, and H.
849 Motoyama (2016), Spatial distributions of soluble salts in surface snow of East Antarctica, *Tellus*
850 *B*, *68*(29285), 1–12, doi:10.3402/tellusb.v68.29285.
851 Iizuka, Y., R. Uemura, H. Motoyama, T. Suzuki, T. Miyake, M. Hirabayashi, and T. Hondoh (2012a),
852 Sulphate-climate coupling over the past 300,000 years in inland Antarctica, *Nature*, *490*(7), 81–84,
853 doi:10.1038/nature11359.
854 Iizuka, Y., S. Horikawa, T. Sakurai, S. Johnson, D. Dahl-Jensen, J. P. Steffensen, and T. Hondoh
855 (2008), A relationship between ion balance and the chemical compounds of salt inclusions found
856 in the Greenland Ice Core Project and Dome Fuji ice cores, *J. Geophys. Res.*, *113*(D7), D07303–
857 07311, doi:10.1029/2007JD009018.

858 Iizuka, Y., T. Miyake, M. Hirabayashi, T. Suzuki, S. Matoba, H. Motoyama, Y. Fujii, and T. Hondoh
859 (2009), Constituent elements of insoluble and non-volatile particles during the Last Glacial
860 Maximum exhibited in the Dome Fuji (Antarctica) ice core, *J. Glaciol.*, *55*(1), 552–562,
861 doi:10.3189/002214309788816696.
862 IPCC (2007), *Climate Change 2007: The Scientific Basis*, Cambridge University Press, U.K., and
863 New York.
864 IPCC (2013), *Climate Change 2013: The Physical Science Basis*, Cambridge, U.K., and New York.
865 Jourdain, B., S. Preunkert, O. Cerri, H. Castebrunet, R. Udisti, R., and M. Legrand (2008),
866 Year-round record of size-segregated aerosol composition in central Antarctica (Concordia
867 station): Implications for the degree of fractionation of sea-salt particles. *J. Geophys. Res.*, *113(D)*,
868 D14308, doi:10.1029/2007JD009584.
869 Jouzel, J. et al. (2007). Orbital and Millennial Antarctic Climate Variability over the Past 800,000
870 Years, *Science*, *317(5)*, 793–796, doi:10.1126/science.1141038.
871 Krinner, G., J. Petit, and B. Delmonte (2010), Altitude of atmospheric tracer transport towards
872 Antarctica in present and glacial climate, *Quat. Sci. Rev.*, *29*, 274–284,
873 doi:10.1016/j.quascirev.2009.06.020.
874 Lambert, F., B. Delmonte, J. R. Petit, M. Bigler, P. R. Kaufmann, M. A. Hutterli, T. F. Stocker, U.
875 Ruth, J. P. Steffensen, and V. Maggi (2008), Dust-climate couplings over the past 800,000years
876 from the EPICA Dome C ice core, *Nature*, *452*(7), 616–619, doi:10.1038/nature06763.
877 Lambert, F., M. Bigler, J. P. Steffensen, M. Hutterli, and H. Fischer (2012), Centennial mineral dust
878 variability in high-resolution ice core data from Dome C, Antarctica, *Clim. Past*, *8*(2), 609–623,
879 doi:10.5194/cp-8-609-2012.
880 Legrand, M. R., and P. Mayewski (1997), Glaciochemistry of polar ice cores: A review, *Rev.*
881 *Geophys.*, *35*(3), 219–243, doi:10.1029/96RG03527
882 Legrand, M. R., C. Hammer, M. De Angelis, J. Savarino, R. Delmas, H. Clausen, and S. J. Johnsen
883 (1997), Sulfur-containing species (methanesulfonate and SO_4^{2-}) over the last climatic cycle in the
884 Greenland Ice Core Project (central Greenland) ice core, *J. Geophys. Res.*, *102*(C12), 26663–
885 26679, doi:10.1029/97JC01436.
886 Legrand, M. R., C. Lorius, N. I. Barkov, and V. N. Petrov (1988), Vostok (Antarctica) ice core -
887 atmospheric chemistry changes over the last climatic cycle (160,000 Years), *Atmos. Environ.*,
888 *22*(2), 317–331, doi:10.1016/0004-6981(88)90037-6.
889 Legrand, M. R., E. Wolff, and D. Wagenbach (1999), Antarctic aerosol and snowfall chemistry:
890 implications for deep Antarctic ice-core chemistry, *Ann. Glaciol.*, *29*, 66–72,
891 doi:10.3189/172756499781821094.

892 Legrand, M. R., S. Preunkert, E. Wolff, R. Weller, B. Jourdain, and D. Wagenbach (2017),
893 Year-round records of bulk and size-segregated aerosol composition in central Antarctica
894 (Concordia site) – Part 1: Fractionation of sea-salt particles, *Atmos. Chem. Phys.*, *17*(2), 14039–
895 14054, doi:10.5194/acp-17-14039-2017.
896 Li, F., P. Ginoux, and V. Ramaswamy (2008), Distribution, transport, and deposition of mineral dust
897 in the Southern Ocean and Antarctica: Contribution of major sources, *J. Geophys. Res. Oceans*,
898 *113*(D10), 573–515, doi:10.1029/2007JD009190.
899 Littot, G. C., R. Mulvaney, R. Röthlisberger, R. Udisti, E. W. Wolff, E. Castellano, M. De Angelis, M.
900 E. Hansson, S. Sommer, and J. P. Steffenssen (2002), Comparison of analytical methods used for
901 measuring major ions in the EPICA Dome C (Antarctica) ice core, *Ann. Glaciol.*, *35*(1), 299–305,
902 doi:10.3189/172756402781817022.
903 Mahalinganathan, K., and M. Thamban (2016), Potential genesis and implications of calcium nitrate
904 in Antarctic snow, *The Cryosphere*, *10*(2), 825–836, doi:10.5194/tc-10-825-2016.
905 Mahowald, N. M., D. R. Muhs, S. Levis, P. J. Rasch, M. Yoshioka, C. S. Zender, and C. Luo (2006),
906 Change in atmospheric mineral aerosols in response to climate: Last glacial period, preindustrial,
907 modern, and doubled carbon dioxide climates. *J. Geophys. Res. Atmos.*, *111(D)*, D10202,
908 doi:10.1029/2005JD006653.
909 Marino, F., E. Castellano, D. Ceccato, P. De Deckker, B. Delmonte, G. Ghermandi, V. Maggi, J. R.
910 Petit, M. Revel-Rolland, and R. Udisti (2008), Defining the geochemical composition of the
911 EPICA Dome C ice core dust during the last glacial-interglacial cycle, *Geochem. Geophys.*
912 *Geosyst.*, *9*(10), Q10018, doi:10.1029/2008GC002023.
913 Martin, J. H., R. M. Gordon, and S. E. Fitzwater (1990), Iron in Antarctic waters, *Nature*, *345*(6),
914 156–158, doi:10.1038/345156a0a.
915 Martínez-Garcia, A., A. Rosell-Melé, S. L. Jaccard, W. Geibert, D. M. Sigman, and G. H. Haug
916 (2011), Southern Ocean dust–climate coupling over the past four million years, *Nature*, *476*(7),
917 312–315, doi:10.1038/nature10310.
918 Millero, F. J., R. Feistel, D. G. Wright, and T. J. McDougall (2008), The composition of standard
919 seawater and the definition of the reference-composition salinity scale, *Deep-Sea Res. I*, 55, 50–
920 72, doi: 10.1016/j.dsr.2007.10.001.
921 zNeff, P. D., and N. A. N. Bertler (2015), Trajectory modeling of modern dust transport to the
922 Southern Ocean and Antarctica, *J. Geophys. Res. Atmos.*, *120*(1), 9303–9322,
923 doi:10.1002/2015JD023304.
924 Newberg, J. T., B. M. Matthew, and C. Anastasio (2005), Chloride and bromide depletions in sea-salt
925 particles over the northeastern Pacific Ocean, *J. Geophys. Res. Atmos.*, *110*(D06209),
926 doi:10.1029/2004JD005446.

927 Niimura, N., K. Okada, X. B. Fan, K. Kai, K. Arao, G. Y. Shi, and S. Takahashi (1998), Formation of
928 Asian dust-storm particles mixed internally with sea salt in the atmosphere, *J. Meteor. Soc. Japan*,
929 *76*(2), 275–288, doi:10.2151/jmsj1965.76.2_275.
930 Nickovic, S., A. Vukovic, M. Vujadinovic, V. Djurdjevic, and G. Pejanovic, (2012), Technical Note:
931 High-resolution mineralogical database of dust-productive soils for atmospheric dust modeling,
932 *Atmos. Chem. Phys.*, 12(2), 845–855, doi:10.5194/acp-12-845-2012.
933 Ohgaito, R., A. Abe-Ouchi, R. O'ishi, T. Takemura, A. Ito, T. Hajima, S. Watanabe, and M.
934 Kawamiya. (2018), Effect of high dust amount on surface temperature during the Last Glacial
935 Maximum: a modelling study using MIROC-ESM, *Clim. Past, 14(1)*, 1565–1581,
936 doi:10.5194/cp-14-1565-2018.
937 Ohno, H., M. Igarashi, and T. Hondoh (2005), Salt inclusions in polar ice core: Location and
938 chemical form of water-soluble impurities, *Earth Planet. Sci. Lett.*, *232*(1–2), 171–178,
939 doi:10.1016/j.epsl.2005.01.001.
940 Ohno, H., M. Igarashi, and T. Hondoh (2006), Characteristics of salt inclusions in polar ice from
941 Dome Fuji, East Antarctica, *Geophys. Res. Lett.*, *33*(8), L08501, doi:10.1029/2006GL025774.
942 Oyabu, I., Y. Iizuka, H. Fischer, S. Schüpbach, G. Gfeller, A. Svensson, M. Fukui, J. P. Steffensen,
943 and M. Hansson (2015), Chemical compositions of solid particles present in the Greenland
944 NEEM ice core over the last 110,000 years, *J. Geophys. Res.*, *120*, 9789–9813,
945 doi:10.1002/2015JD023290.
946 Oyabu, I., Y. Iizuka, R. Uemura, T. Miyake, M. Hirabayashi, H. Motoyama, T. Sakurai, T. Suzuki,
947 and T. Hondoh (2014), Chemical compositions of sulfate and chloride salts over the last
948 termination reconstructed from the Dome Fuji ice core, inland Antarctica, *J. Geophys. Res. Atmos.*,
949 *119*(2), 14045–140058, doi:10.1002/2014JD022030.
950 Parrenin, F., et al. (2016), Climate dependent contrast in surface mass balance in East Antarctica over
951 the past 216 ka, *J. Glaciol.*, *62*(236), 1037–1048, doi:10.1017/jog.2016.85.
952 Petit, J. R., et al. (1999), Climate and atmospheric history of the past 420,000 years from the Vostok
953 ice core, Antarctica, *Nature*, *399*(6735), 429–436, doi:10.1038/20859.
954 Pye, K (1994), Shape sorting during wind transport of quartz silt grains; discussion, *J. Sediment. Res.*
955 *64 (3a)*, 704–705, doi:10.1306/D4267E8D-2B26-11D7-8648000102C1865D.
956 Rankin, A. M. and E. Wolff (2002), Frost flowers: Implications for tropospheric chemistry and ice
957 core interpretation, *J. Geophys. Res. Atmos.*, 107(D23), 4683–17, doi:10.1029/2002JD002492.
958 Revel-Rolland, M., P. De Deckker, B. Delmonte, P. P. Hesse, J. W. Magee, I. Basile-Doelsch, F.
959 Grousset, and D. Bosch (2006), Eastern Australia: A possible source of dust in East Antarctica
960 interglacial ice, *Earth Planet. Sci. Lett.*, *249*(1), 1–13, doi:10.1016/j.epsl.2006.06.028.

961 Röthlisberger, R., M. A. Hutterli, and E. W. Wolff (2002), Nitrate in Greenland and Antarctic ice
962 cores: A detailed description of post-depositional processes, *Ann. Glaciol.*,
963 doi:10.3189/172756402781817220.
964 Röthlisberger, R., M. A. Hutterli, S. Sommer, E. W. Wolff, and R. Mulvaney (2000), Factors
965 controlling nitrate in ice cores: Evidence from the Dome C deep ice core, *J. Geophys. Res.*,
966 *105*(D16), 20565–20572, doi:10.1029/2000jd900264.
967 Röthlisberger, R., R. Mulvaney, E. W. Wolff, M. A. Hutterli, M. Bigler, M. De Angelis, M. E.
968 Hansson, J. P. Steffensen, and R. Udisti (2003), Limited dechlorination of sea-salt aerosols during
969 the last glacial period: Evidence from the European Project for Ice Coring in Antarctica (EPICA)
970 Dome C ice core, *J. Geophys. Res.*, *108*(D), 4526, doi:10.1029/2003JD003604, 2003.
971 Ruth, U., et al. (2008), Proxies and measurement techniques for mineral dust in Antarctic ice cores,
972 *Environ. Sci. Technol.*, *42*(15), 5675–5681, doi:10.1021/es703078z.
973 Sakurai, T., H. Ohno, S. Horikawa, Y. Iizuka, T. Uchida, K. Hirakawa, and T. Hondoh (2011), The
974 chemical forms of water-soluble microparticles preserved in the Antarctic ice sheet during
975 Termination I, *J. Glaciol.*, *57*(206), 1027–1032, doi:10.3189/002214311798843403.
976 Sala, M., et al. (2008), Evidence of calcium carbonates in coastal (Talos Dome and Ross Sea area)
977 East Antarctica snow and firn: Environmental and climatic implications, *Earth Planet. Sci. Lett.*,
978 *271*(1), 43–52, doi:10.1016/j.epsl.2008.03.045.
979 Salter, M. E., E. Hamacher-Barth, C. Leck, J. Werner, C. M. Johnson, I. Riipinen, E. D. Nilsson, and
980 P. Zieger (2016), Calcium enrichment in sea spray aerosol particles, *Geophys. Res. Lett.*, *43*,
981 8277–8285, doi:10.1002/2016GL070275.
982 Sato, H., T. Suzuki, M. Hirabayashi, Y. Iizuka, and H. Motoyama (2013), Mineral and sea-salt
983 aerosol fluxes over the last 340 kyr reconstructed from the total concentration of Al and Na in the
984 Dome Fuji ice core, *Atmos. Clim. Sci.*, *3*, 186–192, doi:10.4236/acs.2013.32020.
985 Savarino, J., J. Kaiser, S. Morin, D. M. Sigman, and M. H. Thiemens (2007), Nitrogen and oxygen
986 isotopic constraints on the origin of atmospheric nitrate in coastal Antarctica, *Atmos. Chem. Phys.*,
987 *7*(8), 1925–1945, doi:10.5194/acp-7-1925-2007.
988 Schindelin, J., et al. (2012). Fiji: an open-source platform for biological-image analysis, *Nature*
989 *Methods*, 9(7), 676–682, doi: 10.1038/nmeth.2019.
990 Siggaard-Andersen, M.-L., P. Gabrielli, J. P. Steffensen, T. Strømfeldt, C. Barbante, C. Boutron, H.
991 Fischer, and H. Miller (2007), Soluble and insoluble lithium dust in the EPICA Dome C ice
992 core—Implications for changes of the East Antarctic dust provenance during the recent glacial–
993 interglacial transition, *Earth Planet. Sci. Lett.*, *258*(1–2), 32–43, doi:10.1016/j.epsl.2007.03.013.

994 Sudarchikova, N., U. Mikolajewicz, C. Timmreck, D. O'Donnell, D., G. Schurgers, D. Sein, and K.
995 Zhang (2015), Modelling of mineral dust for interglacial and glacial climate conditions with a
996 focus on Antarctica, *Clim. Past*, 11(5), 765–779, doi: 10.5194/cp-11-765-2015.
997 Sugden, D. E., R. D. McCulloch, A. J. M. Bory, and A. S. Hein (2009), Influence of Patagonian
998 glaciers on Antarctic dust deposition during the last glacial period, *Nat. Geosci.*, *2*(4), 281–285,
999 doi:10.1038/ngeo474.
1000 Thibert, E., and F. Domine (1997), Thermodynamics and kinetics of the solid solution of HCl in ice,
1001 *J. Phys. Chem. B*, *101*(18), 3554–3565, doi:10.1021/jp962115o.
1002 Udisti, R., S. Becagli, S. Benassai, E. Castellano, I. Fattori, M. Innocenti, A. Migliori, and R.
1003 Traversi (2004), Atmosphere–snow interaction by a comparison between aerosol and uppermost
1004 snow layers composition at Dome Concordia (East Antarctica), *Ann. Glaciol.*, *39*, 53–61,
1005 doi:10.3189/172756404781814474.
1006 Udisti, R., U. Dayan, S. Becagli, M. Busetto, D. Frosini, M. Legrand, F. Lucarelli, S. Preunkert, M.
1007 Severi, R. Traversi, and V. Vitale (2012), Sea spray aerosol in central Antarctica. Present
1008 atmospheric behaviour and implications for paleoclimatic reconstructions, *Atmos. Environ.*, 52,
1009 109–120, doi: 10.1016/j.atmosenv.2011.10.018.
1010 Usher, C. R., A. E. Michel, and V. H. Grassian (2003), Reactions on mineral dust, *Chem. Rev.*,
1011 doi:10.1021/cr020657y.
1012 Vallelonga, P., et al. (2010), Lead isotopic compositions in the EPICA Dome C ice core and Southern
1013 Hemisphere Potential Source Areas, *Quat. Sci. Rev.*, *29*(1–2), 247–255,
1014 doi:10.1016/j.quascirev.2009.06.019.
1015 Veres, D., et al. (2013), The Antarctic ice core chronology (AICC2012): An optimized
1016 multi-parameter and multi-site dating approach for the last 120 thousand years, *Clim. Past*, *9*(4),
1017 1733–1748, doi:10.5194/cp-9-1733-2013.
1018 Vogt, R., P. J. Crutzen, and R. Sander (1996), A mechanism for halogen release from sea-salt aerosol
1019 in the remote marine boundary layer, *Nature*, *383*, 327–330, doi:10.1038/383327a0.
1020 Watanabe, O., J. Jouzel, S. Johnsen, F. Parrenin, H. Shoji, and N. Yoshida (2003b), Homogeneous
1021 climate variability across East Antarctica over the past three glacial cycles, *Nature*, *422*(6), 509–
1022 512, doi:10.1038/nature01525.
1023 Watanabe, O., K. Kamiyama, and H. Motoyama (2003a), General tendencies of stable isotopes and
1024 major chemical constituents of the Dome Fuji deep ice core, *Mem. Natl Inst. Polar Res., Spec.*
1025 *Issue*, *57*.
1026 Wegner, A., P. Gabrielli, D. Wilhelms-Dick, U. Ruth, M. Kriews, P. De Deckker, C. Barbante, G.
1027 Cozzi, B. Delmonte, and H. Fischer (2012), Change in dust variability in the Atlantic sector of

1028 Antarctica at the end of the last deglaciation, *Clim. Past*, *8*(1), 135–147,
1029 doi:10.5194/cp-8-135-2012.
1030 Wessel, P., W. H. F. Smith, R. Scharroo, J. F. Luis, and F. Wobbe, (2013), Generic Mapping Tools:
1031 Improved version released. EOS Trans, AGU, 94, 409–410 (2013).
1032 Wolff, E. W. (1995), *Nitrate in Polar Ice*, 195–224 pp., Springer, Berlin, Heidelberg,
1033 doi:10.1007/978-3-642-51172-1_10.
1034 Wolff, E. W., et al. (2006), Southern Ocean sea-ice extent, productivity and iron flux over the past
1035 eight glacial cycles, *Nature*, *440*(7083), 491–496, doi:10.1038/nature04614.
1036 Wolff, E. W., et al. (2010), Changes in environment over the last 800,000 years from chemical
1037 analysis of the EPICA Dome C ice core, *Quat. Sci. Rev.*, *29*(1–2), 285–295,
1038 doi:10.1016/j.quascirev.2009.06.013.
1039

1040 **Figure captions**

1041 **Figure 1.** Map of ice core sites cited in this study and locations of the potential sources for dust in
1042 the Southern Hemisphere. The map was drawn using the Generic Mapping Tools (Wessel et al.,
1043 2013).

1044 **Figure 2.** Classification scheme of nonvolatile particles. Numbers (%) indicate the number fraction
1045 of particles in each category (red: EDC, blue: DF).

1046 **Figure 3.** Examples of SEM images and EDS spectra of nonvolatile particles. **a** and **b**, images of
1047 typical dust, sea-salt and mixed particles. Crosses on the particles indicate the points of EDS
1048 measurements (beam diameter: 64 nm). **c – e,** EDS spectra of the particles 001 (terrestrial dust), 002
1049 (mixture of dust and sea salt), and 003 (sea salt), respectively. Asterisks denote background peaks
1050 derived from the membrane filter (C, O), filter coating (Pt), and sample mount (Cr).

1051 **Figure 4.** Mass fraction of Na in dust and sea salts, and concentration ratio of $ssNa^+$ to total Na.
1052 Color bars indicate mass fractions of Na derived from sublimation-EDS analysis and lines indicate
1053 ratios of ssNa to Na. Here, $(ssNa/Na)_{subl}$ is the sum of the light blue and dark blue bars,
1054 $(ssNa^+/Na^+)_{Bowen}$ is calculated with $nssNa^+/nssCa^{2+}$ = 0.56 (Bowen, 1979), $(ssNa^+/Na^+)_{Bigler}$ is
1055 calculated with $nssNa^+/nssCa^{2+}$ = 0.94 (Bigler et al., 2006), and ssNa/tNa is calculated with the
1056 crustal ratio of Na to Al (=0.29) (Sato et al., 2013). **a**, Dome C, and **b**, Dome Fuji.

1057 **Figure 5.** Size distribution of all particles, sea salts, mixture of sea salts and dust, and terrestrial dust
1058 in the Holocene, Termination, and LGM. Small panels in the size distribution of sea-salt particles in
1059 the Holocene and Termination show size distribution of Na_2SO_4 (magenta) and NaCl (blue). Red
1060 solid line in each panel shows lognormal fitting curve.

1061 **Figure 6.** Distribution of aspect ratios of sea salts, mixture of sea salts and dust, and terrestrial dust
1062 for the all period. Solid line in each panel shows lognormal fitting curve.

1063 **Figure 7.** Number fractions of **a**, terrestrial dust, **b**, mixture of dust and sea salts, **c**, sea salts, and **d**,
1064 others/unknown (dark colors: EDC core, pale colors: DF core). The 95% confidence interval of all
1065 data plotted in this figure is estimated to be <5 %. **e** – **g** are number fractions of terrestrial dust, a
1066 mixture of sea salts and dust, sea-salt, and others/unknown particles of the LGM (25–18 kyr BP),
1067 Termination (17–12 kyr BP), and Holocene (11–9 kyr BP) for the EDC and DF cores.

1068 **Figure 8.** Number fractions of $CaSO_4$, $CaCl_2$, and Ca_{only} particles. **a**, EDC and **b**, DF. Dark blue:
1069 particles containing Ca without Si, S and Cl, dark orange: atomic ratio of S/Ca is 1, pale orange:
1070 atomic ratio of S/Ca is < 1, dark pink: atomic ratio of Cl/Ca is 2, pale pink: atomic ratio of Cl/Ca is <
1071 2, and sky blue: particles containing both $CaSO_4$ and $CaCl_2$.

Figure 9. Fractions of the atomic ratios of Na, S, and Cl in individual sea-salt particles (open circles). Also shown are the fractions of fully modified sea salt by nitric acid ($NaNO_3$, blue closed circles), sulfuric acid (Na_2SO_4, red closed circles), and methanesulfonic acid (CH_3SO_3Na, green closed circles), and initial sea salts from seawater and sea-ice surface (purple closed circles). Note that the initial sea salt from seawater and sea-ice surface have similar fractions and thus indistinguishable on the figure (Millero et al., 2008; Rankin and Wolff, 2002; Hara et al., 2017).

Figure 10. The fraction of Cl in the total number of Na, S, and Cl atoms for individual sea-salt particles (crosses) except for data with Cl = 0, which are shown by open circles (circle area is proportional to the fraction of number of particles). Samples without particles with Cl = 0 are denoted by pluses on zero line. Black and blue dashed lines indicate Cl fractions for sea salts from seawater (Millero et al., 2008) and sea ice (Rankin and Wolff, 2002; Hara et al., 2017), respectively, with uncertainty range (gray shading).

Figure 11. Fluxes of $ssNa^+$, $nssNa^+$, and $nssCa^{2+}$. **a**, $ssNa^+$ flux calculated with $nssNa^+/nssCa^{2+}$ = 0.56 (Bowen, 1979) (red: EDC, blue: DF), **b**, $nssNa^+$ flux calculated with $nssNa^+/nssCa^{2+}$ = 0.56 (Bowen, 1979) (red: EDC, blue: DF), and **c**, $nssCa^{2+}$ flux calculated with $ssNa^+/ssCa^{2+}$ = 23 (Bigler et al., 2006) (red: EDC, blue: DF. ssNa and nssNa fluxes estimated from the sublimation data are represented in **a** and **b**, respectively (open circle with orange: EDC, open square with green: DF).

Figure 12. Modeled dust deposition flux for the LGM from an earth system model, MIROC-ESM (data from Ohgaito et al., 2018).

1093 **Table 1.** *Sizes of Particles Analyzed in the Dome C and Dome Fuji Cores.*

		EDC			DF		
		Median (μm)	Mode (μm)	σ_g (μm)	Median (μm)	Mode (μm)	σ_g (μm)
Holocene (9-11 kyr BP)	All	1.83	1.56	1.60	2.26	1.70	1.76
	Dust	1.85	1.56	1.59	2.26	1.70	1.72
	Mix	1.97	1.56	1.67	2.72	2.28	1.74
	Sea salts	1.71	1.56	1.57	1.62	1.32	1.77
Termination (12-17 kyr BP)	All	1.75	1.51	1.62	2.31	1.80	1.72
	Dust	1.74	1.46	1.65	2.50	1.90	1.72
	Mix	1.91	1.56	1.65	2.35	1.80	1.73
	Sea salts	1.68	1.46	1.55	1.92	1.70	1.61
LGM (18-25 kyr BP)	All	1.75	1.41	1.64	2.39	1.99	1.58
	Dust	1.66	1.36	1.65	2.36	1.94	1.60
	Mix	1.94	1.56	1.63	2.58	2.18	1.53
	Sea salts	1.50	1.36	1.48	1.60	1.51	1.34

1094 Note: σ_g represents geometric standard deviation.

1095

1096 **Table 2.** *Aspect Ratios of Particles Analyzed in the Dome C and Dome Fuji Cores.*

		EDC Mode	DF Mode
Holocene (9-11 kyr BP)	Dust	1.40	1.38
	Mix	1.36	1.36
	Sea salts	1.36	1.36
Termination (12-17 kyr BP)	Dust	1.42	1.38
	Mix	1.40	1.40
	Sea salts	1.36	1.38
LGM (18-25 kyr BP)	Dust	1.42	1.38
	Mix	1.40	1.40
	Sea salts	1.42	-
All period (9-25 kyr BP)	Dust	1.42	1.38
	Mix	1.38	1.38
	Sea salts	1.36	1.36

1097

1098

1099 **Table 3.** *Average Fluxes of sea-salt (ss) Na and non-sea-salt (nss) Na in the Dome C Core and their Ratios*
1100 *with the Dome Fuji Core*

1101

	EDC flux[a,b] (mg m^{-2} yr^{-1})		DF flux[c] (mg m^{-2} yr^{-1})		DF/EDC flux ratio	
	9-11 kyr BP	18-25 kyr BP	9-11 kyr BP	18-25 kyr BP	9-11 kyr BP	18-25 kyr BP
$ssNa^+_{Bigler}$[d]	0.40	0.80	0.55	0.77	1.38	0.96
$ssNa^+_{Bowen}$[e]	0.42	1.03	0.58	1.11	1.38	1.08
$ssNa^+_{subl}$[f]	0.48	1.05	0.46	1.07	0.96	1.02
$nssNa^+_{Bigler}$[d]	0.02	0.54	0.07	0.84	3.50	1.56
$nssNa^+_{Bowen}$[e]	0.01	0.32	0.04	0.49	4.00	1.53
$nssNa^+_{subl}$[f]	0.03	0.31	0.30	0.51	10.0	1.65

1102

1103 Note: Na^+ flux is divided into $ssNa^+$ and $nssNa^+$ using published ion data ([a]Littot et al., 2002; [b]Wolff et al.,
1104 2006; [c]Oyabu et al., 2014) with $nssNa^+/nssCa^{2+}$ ([d]Bigler et al., 2006 or [e]Bowen, 1979) or with ssNa/Na from
1105 the particle classification after sublimation ([f]this study). The values from the different methods are denoted by
1106 subscript letters. The DF/EDC flux ratios are calculated for the respective methods and periods.
1107

1108 **Table 4** Average concentrations of six ion species in the early Holocene and LGM for the EDC[a] and DF[b, c]
1109 cores.

	Age	Cl^-	NO_3^-	SO_4^{2-}	Na^+	Mg^{2+}	Ca^{2+}
EDC	early Holocene (9 – 11 kyr BP)	0.78[a]	0.21[a]	1.00[a]	0.77[a]	0.10[a]	0.17[a]
EDC	LGM (18 – 25 kyr BP)	5.17[a]	0.81[a]	2.18[a]	4.71[a]	0.79[a]	1.10[a]
DF	early Holocene (9 – 11 kyr BP)	1.31[b]	0.39[c]	1.03[b]	0.95[b]	0.11[b]	0.10[b]
DF	LGM (18 – 25 kyr BP)	4.82[b]	1.88[c]	2.17[b]	4.37[b]	0.77[b]	1.59[b]

1110 Note: [a]Littot et al. (2002), [b]Oyabu et al. (2014), [c]Goto-Azuma et al. (2019). Unit is μmol l^{-1}.

Figure 1.

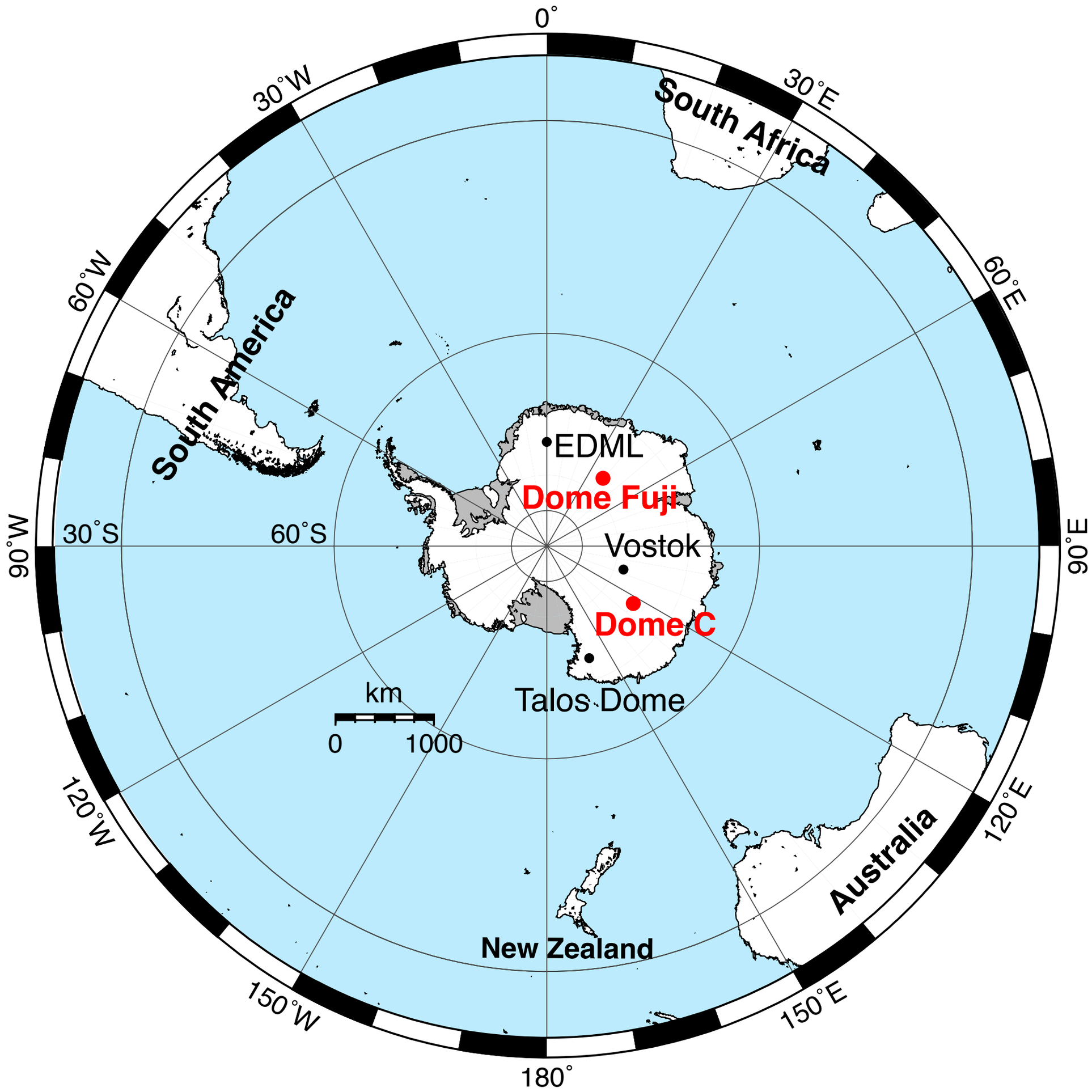
0°
30°W
30°E
60°W
60°E
90°W
90°E
120°W
120°E
150°W
150°E
180°
30°S
60°S
South Africa
South America
Australia
New Zealand
EDML
Dome Fuji
Vostok
Dome C
Talos Dome
km
0
1000

Figure 2.

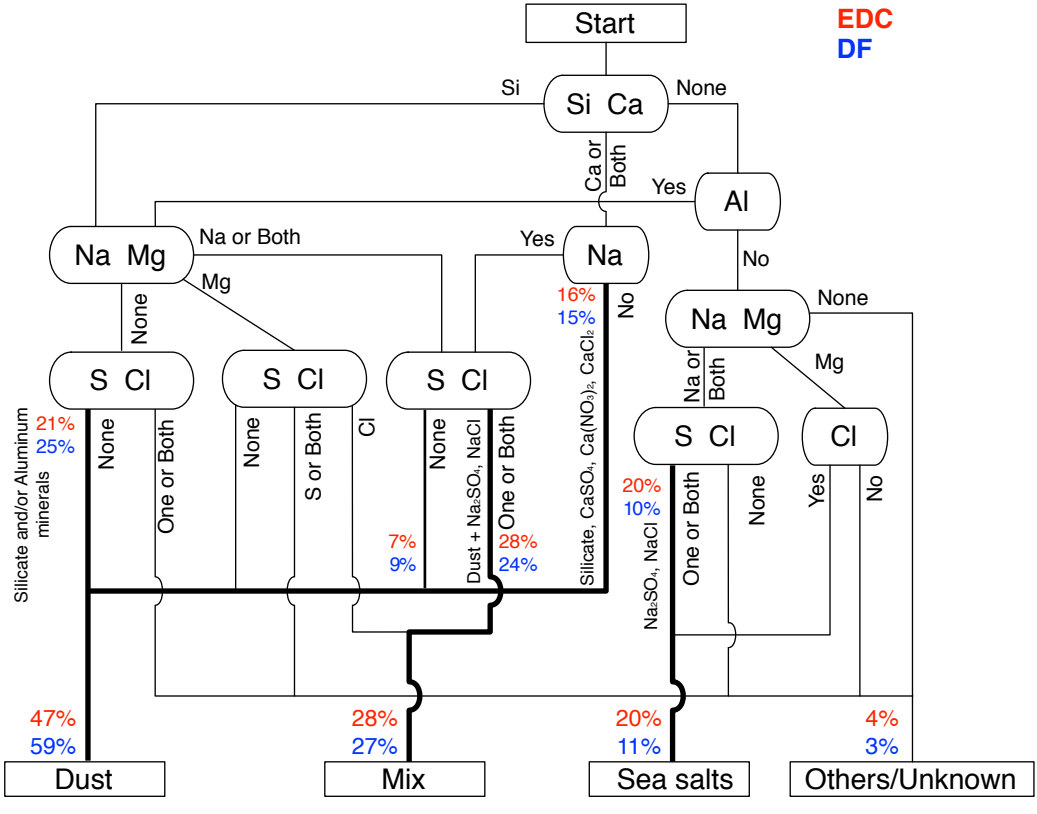
EDC
DF
Start
Si
Si Ca
None
Ca or Both
Yes
Al
Na Mg
Na or Both
Mg
None
Yes
Na
No
16%
15%
Na Mg
None
Mg
Na or Both
S Cl
S Cl
S Cl
S Cl
Cl
21%
25%
None
One or Both
None
S or Both
Cl
None
One or Both
Silicate and/or Aluminum minerals
7%
9%
28%
24%
Dust + Na2SO4, NaCl
Silicate, CaSO4, Ca(NO3)2, CaCl2
20%
10%
Na2SO4, NaCl
One or Both
None
Yes
No
47%
59%
28%
27%
20%
11%
4%
3%
Dust
Mix
Sea salts
Others/Unknown

Figure 3.

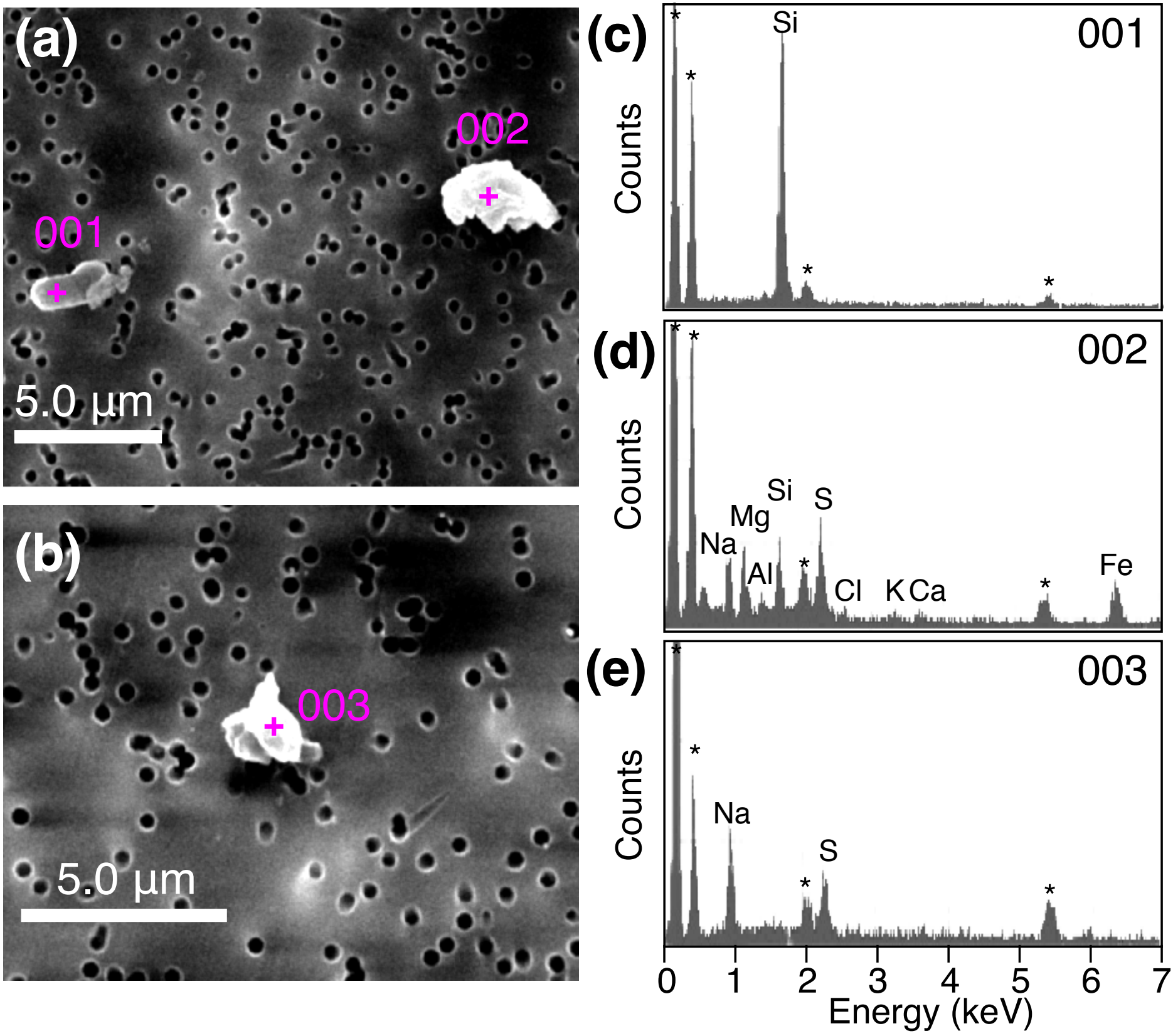
(a)
002
001
5.0 µm
(b)
003
5.0 µm
(c)
001
Si
Counts
(d)
002
Si
S
Mg
Na
Al
Cl
K
Ca
Fe
Counts
(e)
003
Na
S
Counts
0
1
2
3
4
5
6
7
Energy (keV)

Figure 4.

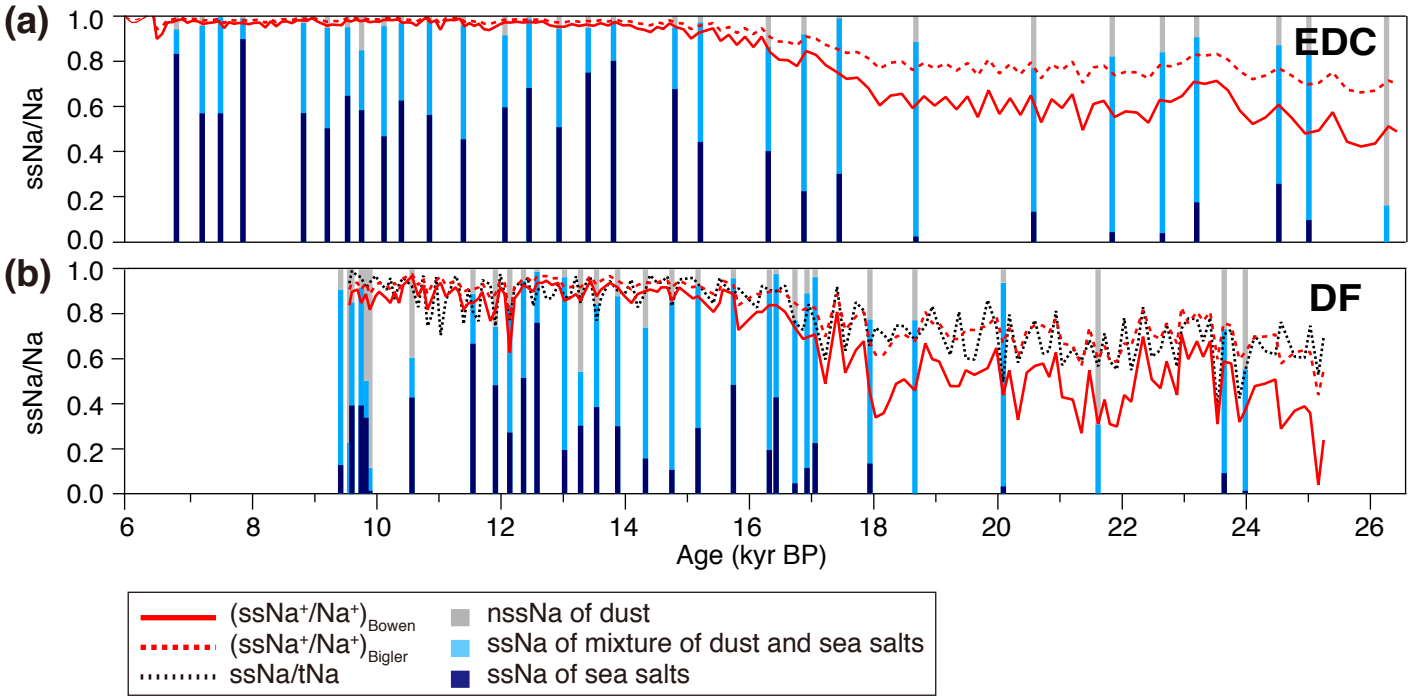
(a)
EDC
ssNa/Na
1.0
0.8
0.6
0.4
0.2
0.0
(b)
DF
ssNa/Na
1.0
0.8
0.6
0.4
0.2
0.0
6
8
10
12
14
16
18
20
22
24
26
Age (kyr BP)
(ssNa+/Na+)Bowen
(ssNa+/Na+)Bigler
ssNa/tNa
nssNa of dust
ssNa of mixture of dust and sea salts
ssNa of sea salts

Figure 5.

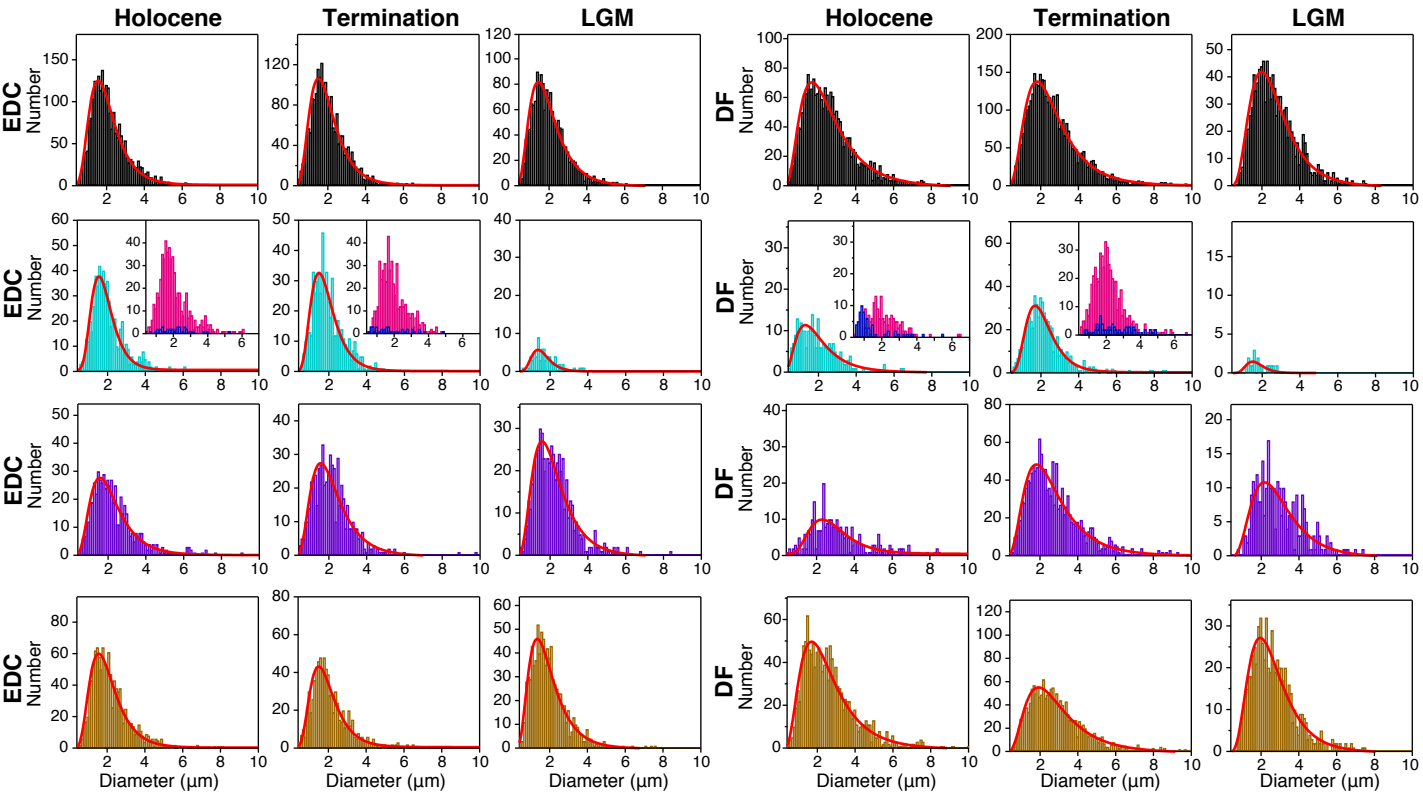
Holocene
Termination
LGM
Holocene
Termination
LGM
EDC
DF
Number
Diameter (μm)
All
Sea salts
Mixture of dust and sea salts
Terrestrial dust
Na_2SO_4
NaCl

Figure 6.

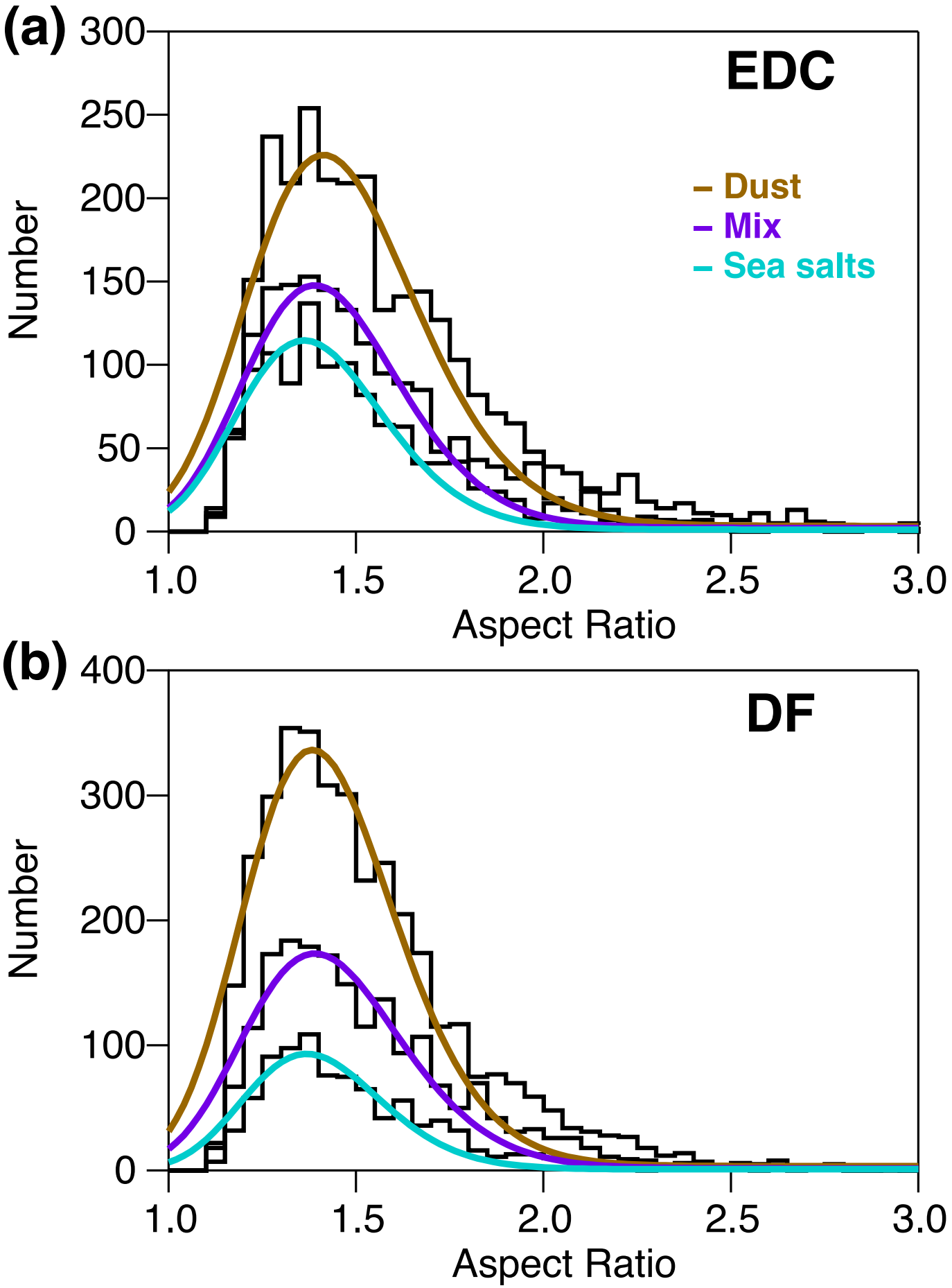
(a)
EDC
Dust
Mix
Sea salts
Number
300
250
200
150
100
50
0
1.0
1.5
2.0
2.5
3.0
Aspect Ratio
(b)
DF
Number
400
300
200
100
0
1.0
1.5
2.0
2.5
3.0
Aspect Ratio

Figure 7.

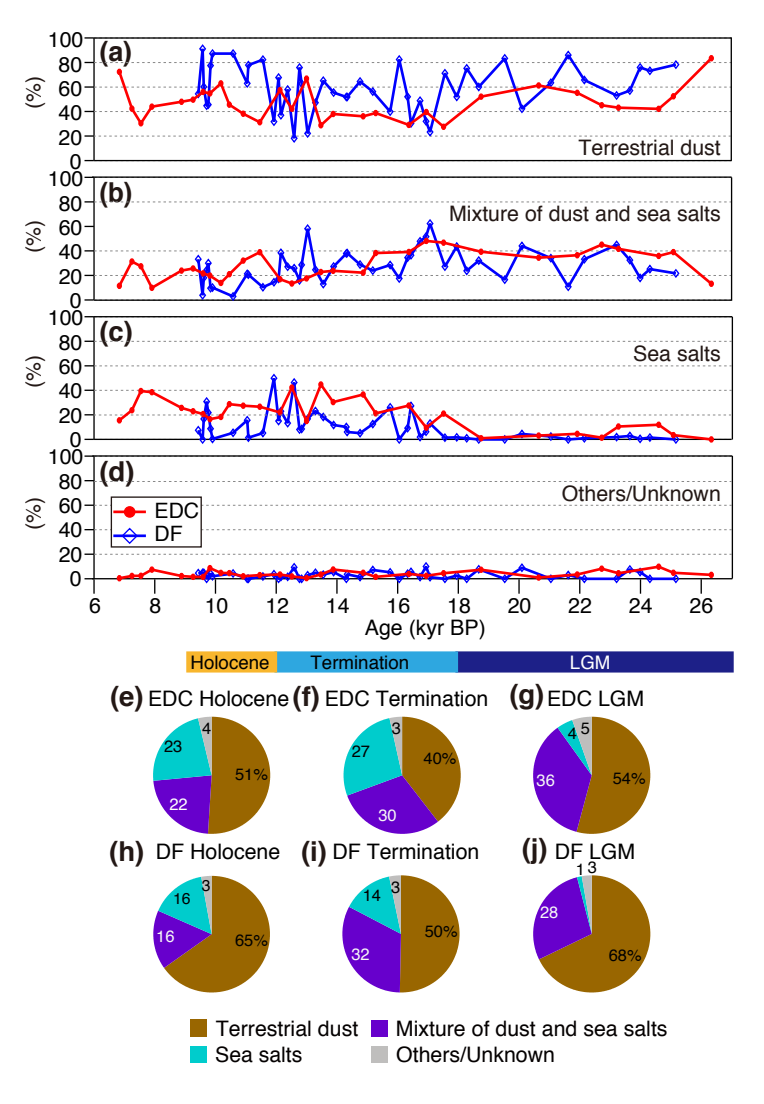
(a)
Terrestrial dust
(b)
Mixture of dust and sea salts
(c)
Sea salts
(d)
Others/Unknown
EDC
DF
(%)
Age (kyr BP)
Holocene
Termination
LGM
(e) EDC Holocene
(f) EDC Termination
(g) EDC LGM
(h) DF Holocene
(i) DF Termination
(j) DF LGM
Terrestrial dust
Mixture of dust and sea salts
Sea salts
Others/Unknown

Figure 8.

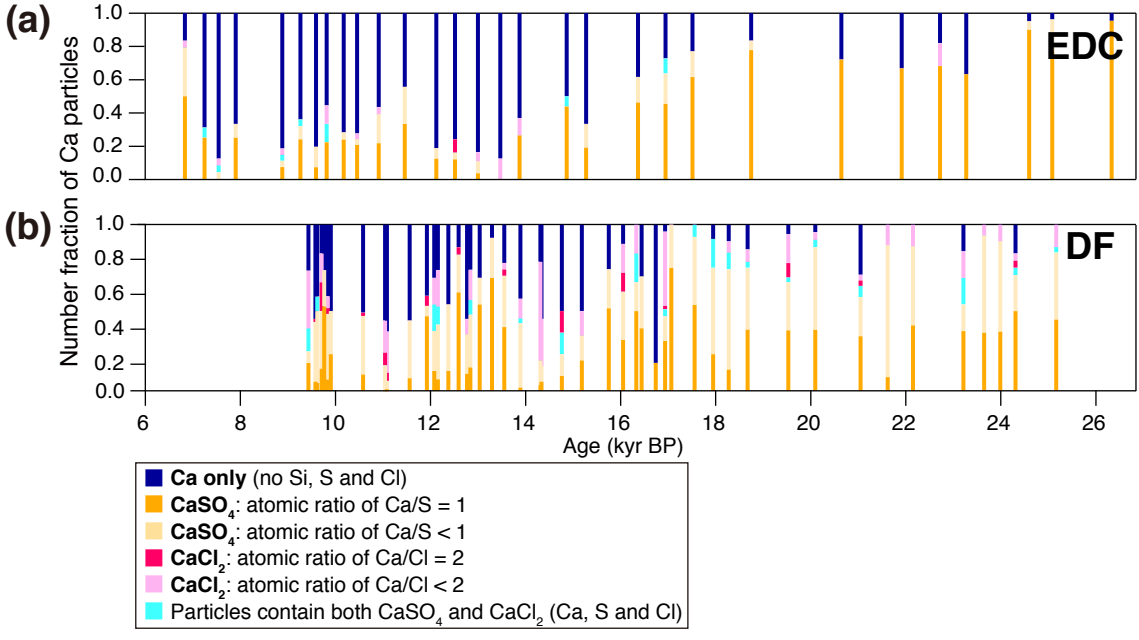
(a)
(b)
EDC
DF
Number fraction of Ca particles
1.0
0.8
0.6
0.4
0.2
0.0
6
8
10
12
14
16
18
20
22
24
26
Age (kyr BP)
Ca only (no Si, S and Cl)
CaSO4: atomic ratio of Ca/S = 1
CaSO4: atomic ratio of Ca/S < 1
CaCl2: atomic ratio of Ca/Cl = 2
CaCl2: atomic ratio of Ca/Cl < 2
Particles contain both CaSO4 and CaCl2 (Ca, S and Cl)

Figure 9.

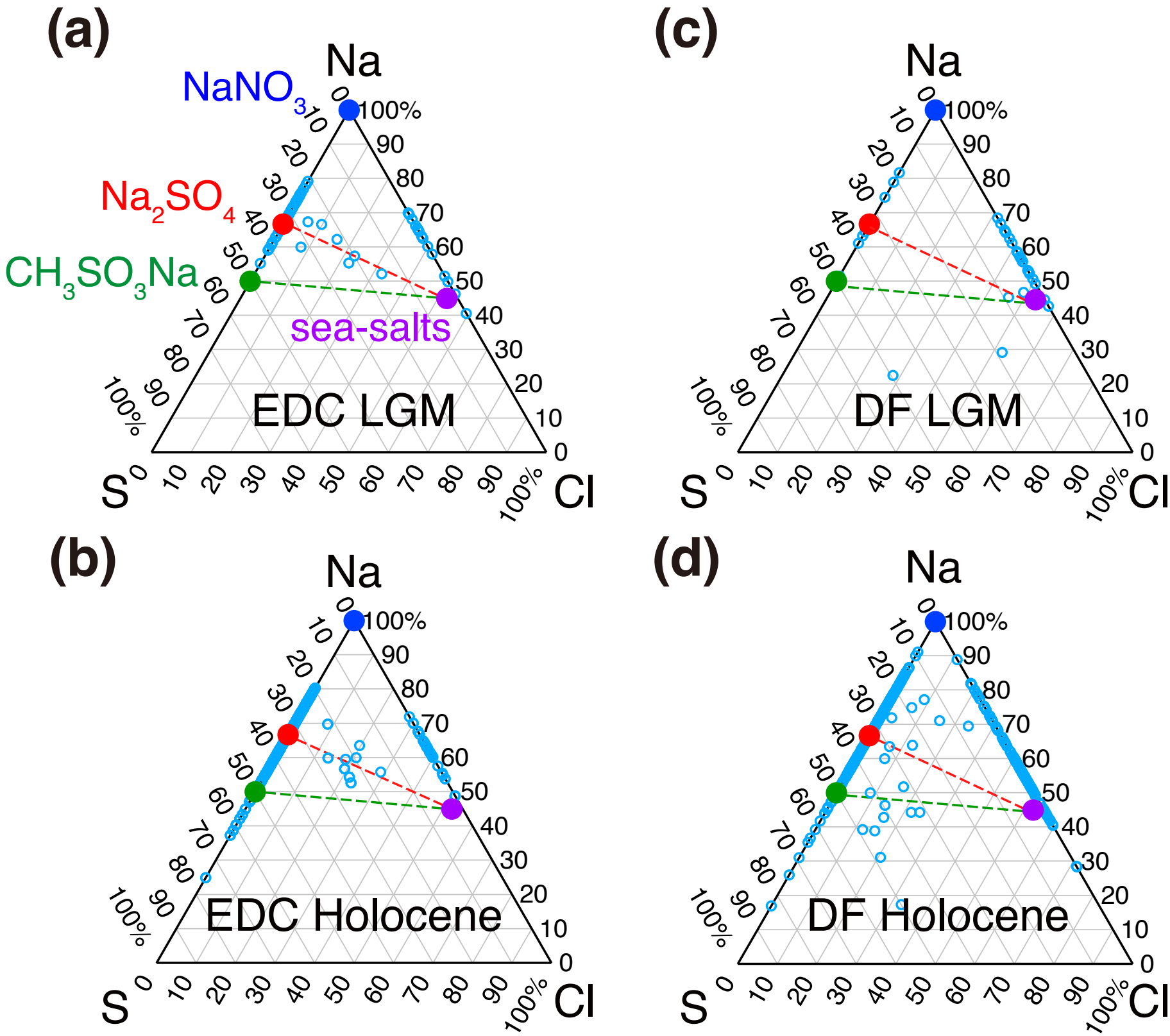
(a)
Na
$NaNO_3$
Na_2SO_4
CH_3SO_3Na
sea-salts
EDC LGM
S
Cl
(c)
Na
DF LGM
S
Cl
(b)
Na
EDC Holocene
S
Cl
(d)
Na
DF Holocene
S
Cl

Figure 10.

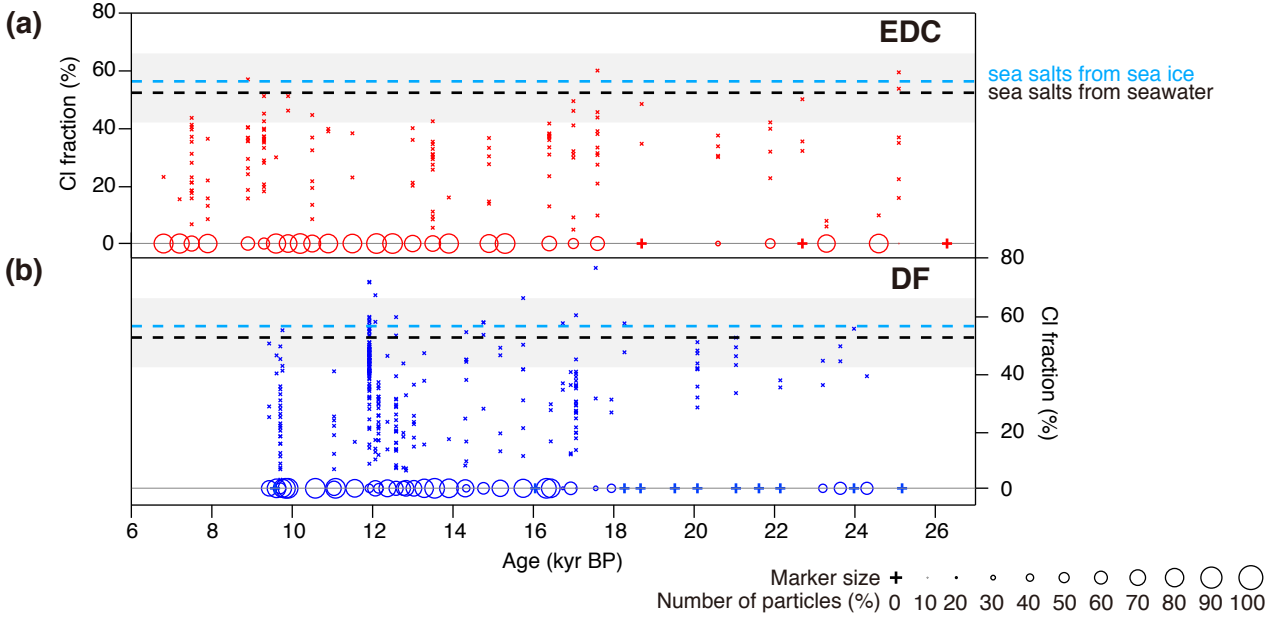
(a)
EDC
(b)
DF
Cl fraction (%)
sea salts from sea ice
sea salts from seawater
Age (kyr BP)
Marker size
Number of particles (%) 0 10 20 30 40 50 60 70 80 90 100

Figure 11.

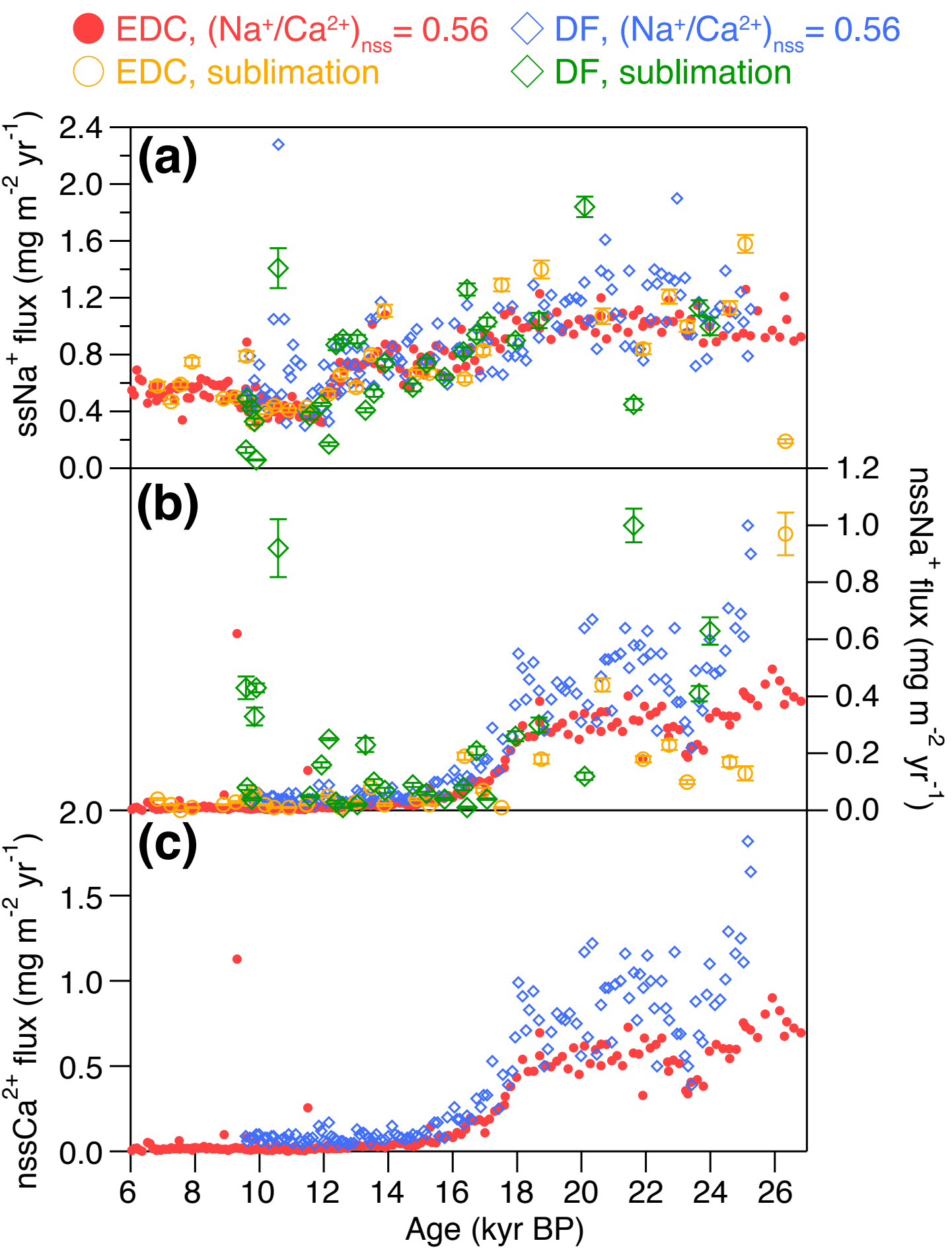
EDC, (Na+/Ca2+)nss= 0.56
DF, (Na+/Ca2+)nss= 0.56
EDC, sublimation
DF, sublimation
(a)
(b)
(c)
ssNa+ flux (mg m-2 yr-1)
nssNa+ flux (mg m-2 yr-1)
nssCa2+ flux (mg m-2 yr-1)
Age (kyr BP)
0.0
0.4
0.8
1.2
1.6
2.0
2.4
0.2
0.6
1.0
0.5
1.5
6
8
10
12
14
16
18
20
22
24
26

Figure 12.

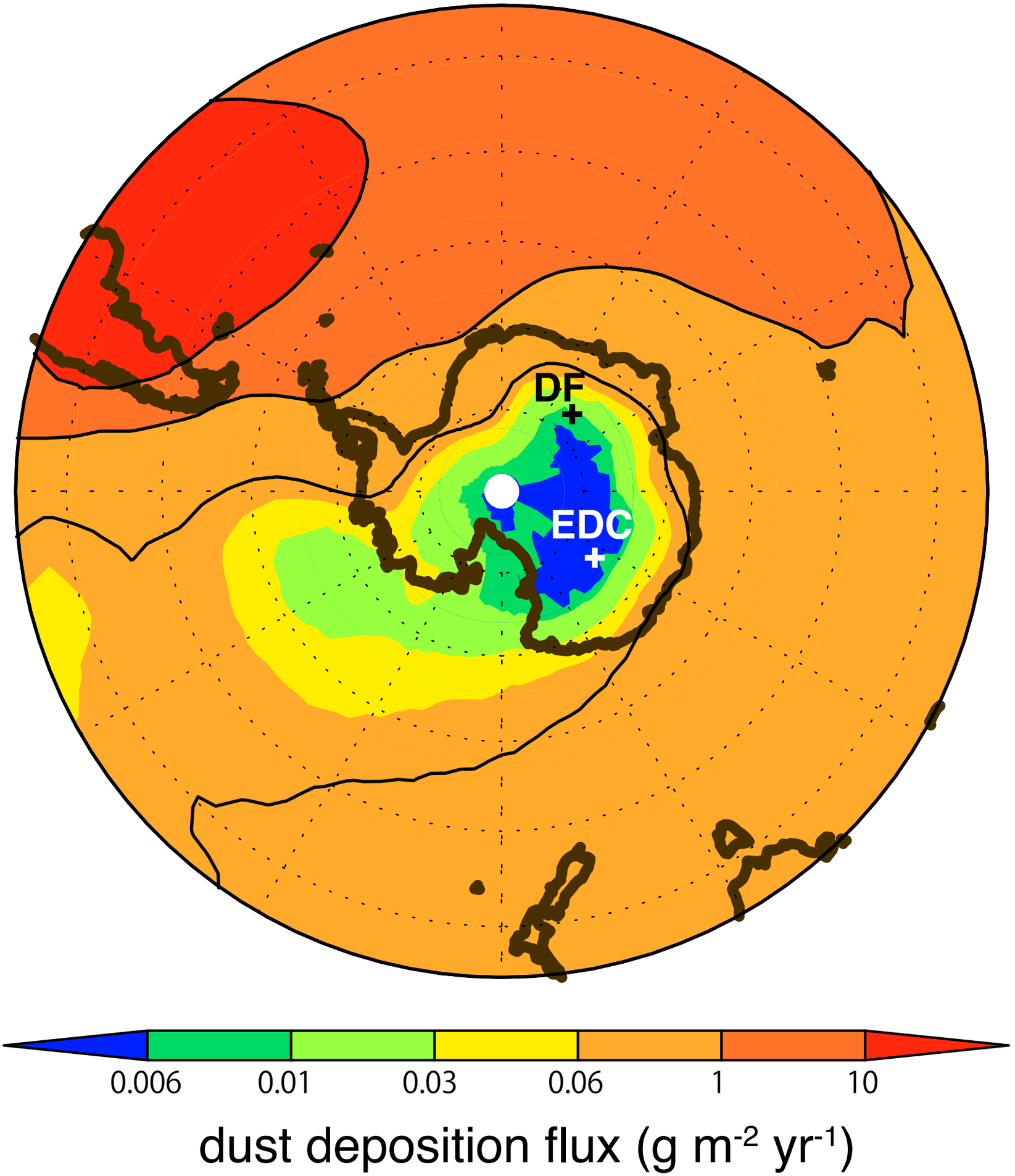
DF
EDC
0.006
0.01
0.03
0.06
1
10
dust deposition flux (g m-2 yr-1)

Appendix Figure 1.

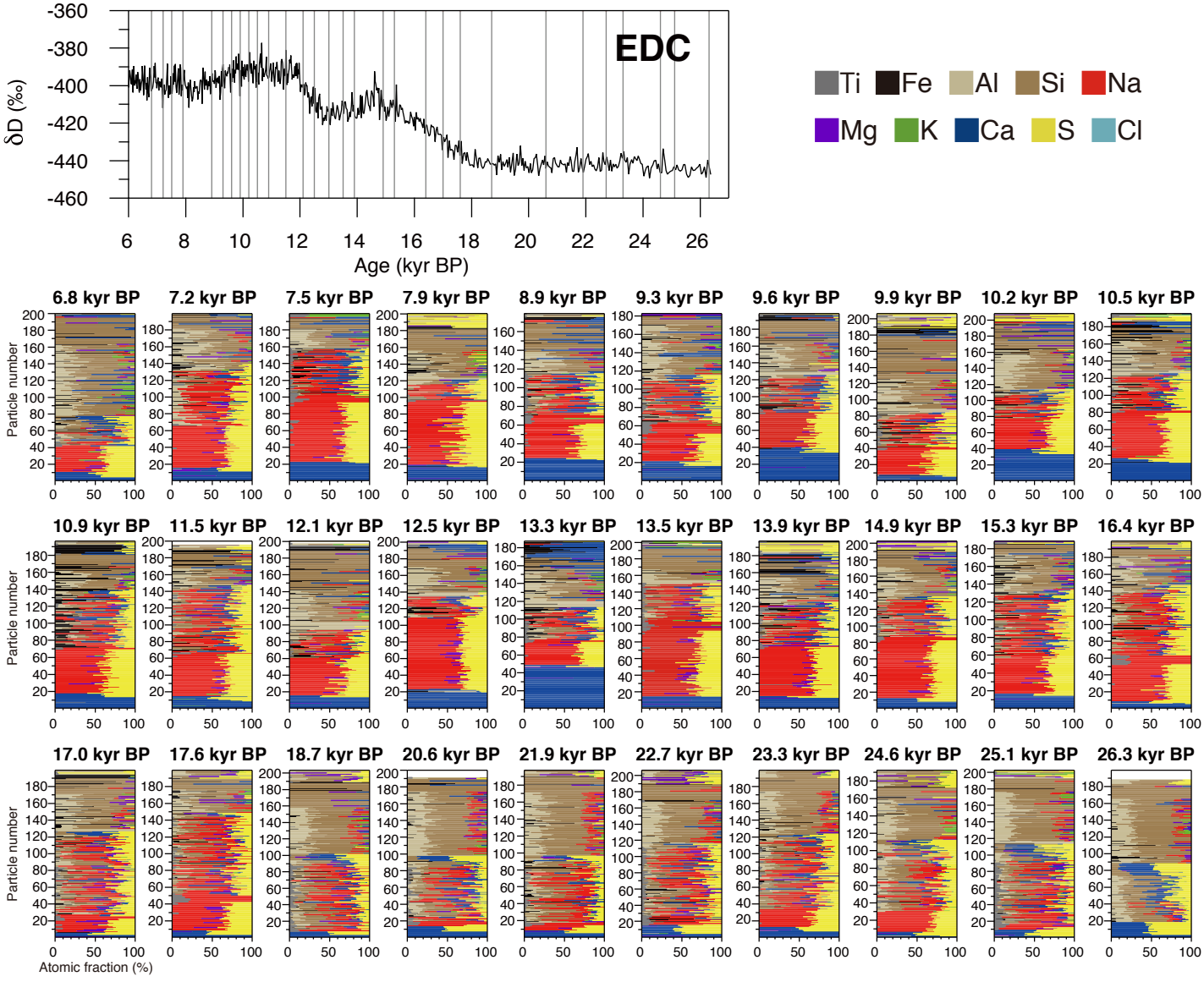
EDC
δD (‰)
-360
-380
-400
-420
-440
-460
6
8
10
12
14
16
18
20
22
24
26
Age (kyr BP)
Ti
Fe
Al
Si
Na
Mg
K
Ca
S
Cl
6.8 kyr BP
7.2 kyr BP
7.5 kyr BP
7.9 kyr BP
8.9 kyr BP
9.3 kyr BP
9.6 kyr BP
9.9 kyr BP
10.2 kyr BP
10.5 kyr BP
10.9 kyr BP
11.5 kyr BP
12.1 kyr BP
12.5 kyr BP
13.3 kyr BP
13.5 kyr BP
13.9 kyr BP
14.9 kyr BP
15.3 kyr BP
16.4 kyr BP
17.0 kyr BP
17.6 kyr BP
18.7 kyr BP
20.6 kyr BP
21.9 kyr BP
22.7 kyr BP
23.3 kyr BP
24.6 kyr BP
25.1 kyr BP
26.3 kyr BP
Particle number
Atomic fraction (%)

Appendix Figure 2.

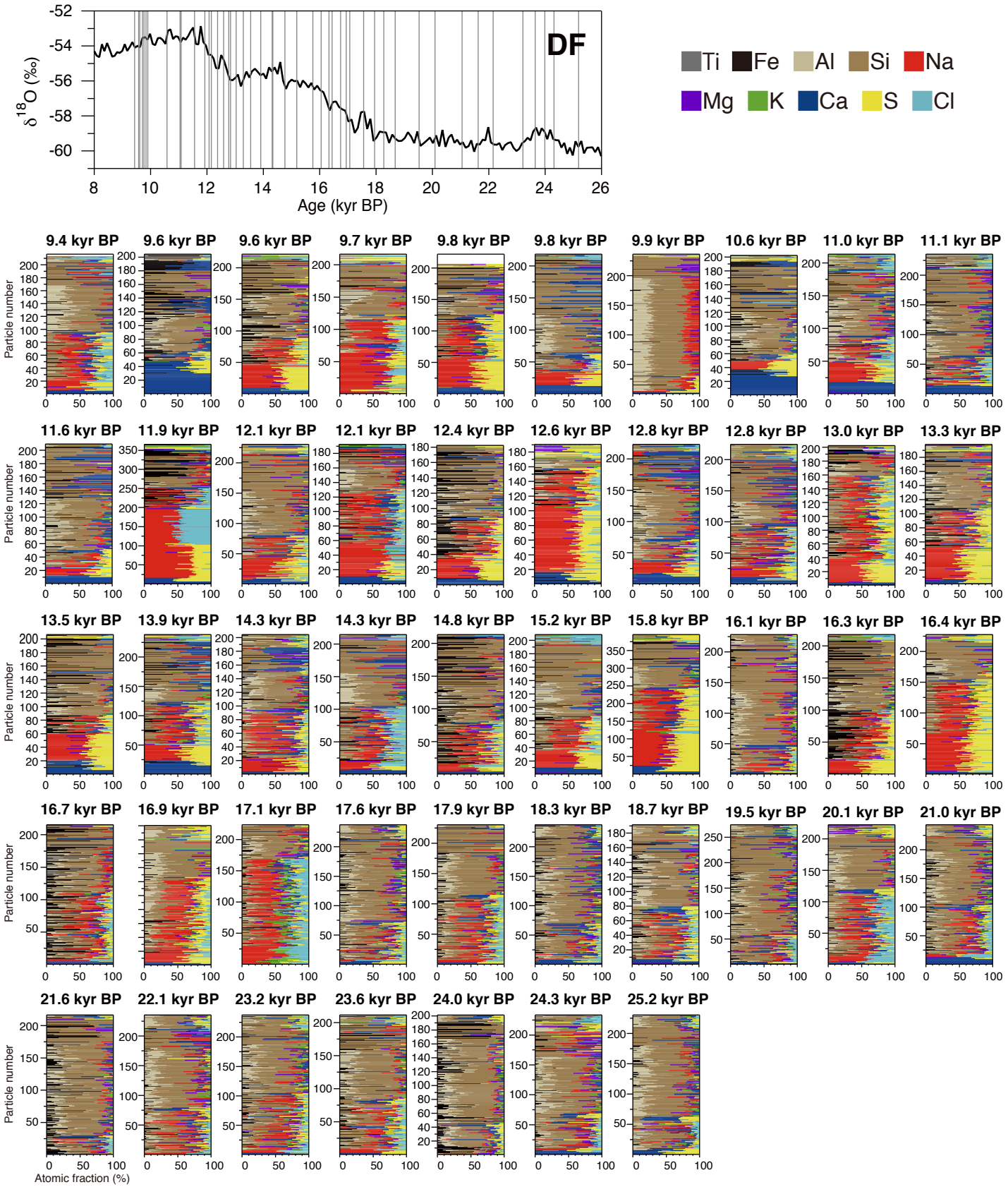
DF
δ18O (‰)
Age (kyr BP)
Ti Fe Al Si Na
Mg K Ca S Cl
9.4 kyr BP
9.6 kyr BP
9.6 kyr BP
9.7 kyr BP
9.8 kyr BP
9.8 kyr BP
9.9 kyr BP
10.6 kyr BP
11.0 kyr BP
11.1 kyr BP
11.6 kyr BP
11.9 kyr BP
12.1 kyr BP
12.1 kyr BP
12.4 kyr BP
12.6 kyr BP
12.8 kyr BP
12.8 kyr BP
13.0 kyr BP
13.3 kyr BP
13.5 kyr BP
13.9 kyr BP
14.3 kyr BP
14.3 kyr BP
14.8 kyr BP
15.2 kyr BP
15.8 kyr BP
16.1 kyr BP
16.3 kyr BP
16.4 kyr BP
16.7 kyr BP
16.9 kyr BP
17.1 kyr BP
17.6 kyr BP
17.9 kyr BP
18.3 kyr BP
18.7 kyr BP
19.5 kyr BP
20.1 kyr BP
21.0 kyr BP
21.6 kyr BP
22.1 kyr BP
23.2 kyr BP
23.6 kyr BP
24.0 kyr BP
24.3 kyr BP
25.2 kyr BP
Particle number
Atomic fraction (%)